Tensile Stress and Thermal Effects on the Grain Boundary Motion in Nanocrystalline Nickel

Somadatta Mohanty

Thesis submitted to the faculty of the Virginia Polytechnic Institute and State University in partial fulfillment of the requirements for the degree of

Master of Science
In
Materials Science and Engineering

Diana Farkas, Chair
Sean G. Corcoran
William T. Reynolds

December 13, 2005
Blacksburg, Virginia

Keywords: tensile stress, thermal grain growth, grain boundary motion, grain boundary sliding, grain rotation

Tensile Stress and Thermal Effects on the Grain Boundary Motion of Nanocrystalline Nickel

Somadatta Mohanty

Abstract

We report on two studies that involve molecular dynamics (MD) simulations of grain boundary motion in nanocrystalline (nc) nickel. The first study is conducted to examine the effects of an applied tensile stress on the grain boundary motion in 5 nm3 nc-Ni specimens, half of which contain free surfaces, while the other half have periodic boundary conditions. Grain boundary sliding (GBS) and grain rotation are the deformation mechanisms exhibited by the nc-Ni specimens, in contrast to dislocation-mediated deformation mechanisms found in bulk samples. Specimens that contain free surfaces display a lower yield stress and a lower average grain boundary velocity compared to their periodic counterparts. These phenomena are attributed to the higher degree of grain boundary sliding present within the free surface specimens.
The second study examines thermal effects of various annealing temperatures on grain boundary motion in 5 nm^3 periodic nc-Ni specimens. It is found that grain growth exhibits a linear relationship with time, as opposed to parabolic grain growth observed in bulk metals. During the annealing process, it is also observed that the average grain boundary energy decreases with $t^{1/2}$, as grains oriented themselves in a lower-energy configuration with their neighbors via grain rotation. An Arrhenius plot of average grain boundary velocity and energy per atom within a grain boundary displays identical slopes, and thus, identical activation energies of ~ 53 kJ for both characteristics. This can be attributed to the fact that grain boundary velocity and energy per atom are governed by the same entity, which is grain boundary diffusion. The annealed samples display a grain rotation-coalescence growth mechanism, where adjacent grains rotate concurrently, to decrease the misorientation energy of the grain boundary between them. It is observed that some grains have achieved the same orientation at the end of the growth process, indicating that the grain boundary has been annihilated, and the two grains have coalesced into a single larger grain.

Acknowledgements

I would like to thank my advisor, Dr. Diana Farkas, for allowing me to work with her and for her guidance and support during my graduate career at Virginia Tech. She has continued to push me to achieve my goals in life. For this, I will be forever grateful.

I would like to especially thank my research partner (in crime), Mr. Joshua Monk (JP), as it was his programming prowess and tutelage that made my graduate research possible. My work is as much his as it is mine. He also deserves my gratitude for being a great friend. Mr. Donald Ward, my favorite student from Brown University, should also be acknowledged for creating a very useful program for my research and also for being a swell fellow. I would like to thank Josh, Don, Mr. Douglas Crowson, and Mr. Arun Nair, for putting up with my eccentric/neurotic/downright-odd behavior and shenanigans. Ms. Emily Sarver also deserves recognition for helping me to format my thesis.

I would like to extend my gratitude to Dr. William Reynolds and Dr. Sean Corcoran for taking time out of their busy schedules and agreeing to be on my committee. I would also like to thank Dr. Marie Paretti for reviewing my thesis and for cheering me on as I turned things around.

My brother and the men I consider my brothers have my deepest respect and gratitude for believing in me and always being there when I needed help.

To Ma and Bapa, I am grateful for your support during the rough times and that you could finally see me perform at a level I had only dreamt of. I could not have done any of this without you. I hope by now, I have made you both very proud.

Lastly, I would like to extend my gratitude to my department head, Dr. David Clark, for believing in me when most people did not. Thank you for your unwavering support, advice on school, and most importantly, your advice on life.

Table of Contents

List of Figures

List of Tables

1. Introduction

In recent decades, nanocrystalline (nc) metals and alloys, with an average grain size less than 100 nm, have been the subject of considerable research. Such interest has been sparked by the discovery of appealing mechanical properties exhibited by nc metals such as high strength, high wear resistance, increasing strength and/or ductility with increasing strain rate, potential for augmented plastic formability at low temperatures, and faster strain rates. This high level of research activity has been facilitated by the advent of new technologies in the fabrication of materials as well as major advances in computational materials science, especially molecular dynamics (MD) simulations, which can be attributed to drastic improvements in computer hardware and software.

1.1 Tensile Stress Effects and Grain Boundary Motion

Mechanical properties of nc metals are not only related to average grain size, D, but also to the distribution of grain sizes, and grain boundary structure (i.e., low-angle versus high-angle grain boundaries). One attribute, strength, has been traditionally expected to increase with the decrease in D, according to the Hall-Petch relationship. However, it has been found that below a certain grain size, ~ 10 nm, strength of an nc metal will decrease with grain size refinement. It is this region that has generated much discussion concerning the mechanical behavior of nc metals. While it is widely accepted that in bulk materials, with $D > 100$ nm, mechanical deformation is facilitated through dislocation mechanisms, mechanical deformation at the nano-scale is not as well understood. Current research seems to indicate that the deformation mechanisms in nc

metals are grain boundary sliding, grain boundary rotation, and motion of partial dislocations.

Compared to bulk metals, nc metals contain a higher fraction of grain boundary volume. For example, for a grain size of 10 nm, it has been found that approximately 14-27% of all the atoms are present within 0.5-1.0 nm of a grain boundary[2]. Thus, grain boundaries are thought to have a major role in mechanical deformation in nc metals. Grain boundaries act as sources and sinks for dislocations and accommodate stress through grain boundary sliding and rotation.

1.2 Thermal Effects and Grain Boundary Motion

Grain growth in metals is thermodynamically-driven by the excess energy of a polycrystalline sample with respect to its single-crystalline form. This energy is manifested through total grain boundary area reduction, resulting in increasing average grain size, D. Classical models of grain growth dictate that the growth rate of D depends strongly on temperature, defect concentrations, second-phase precipitates, and separation and transport of impurity atoms to grain boundary cores. These models follow a parabolic relationship with annealing time.

While these models have been found to be consistent for bulk metals, $D > 1$ μm, they do not seem to apply to nc metals, $D < 100$ nm, where in many studies, grain growth exhibits a linear relationship with annealing time. In coarse-grained materials, grain boundary migration is facilitated through boundary-curvature-driven-diffusion along grain boundary cores[3]. However, in nc metals, it appears that grain boundary migration is related to excess volume within grain boundary cores, grain rotation, and triple

junction migration. Like mechanical deformation, grain growth is not fully understood in nc metals.

1.3 Molecular Dynamics

At such small grain sizes, it is difficult to examine grain boundary behavior without nonintrusive methods when performing experimental measurements. For example, using transmission electron microscopy (TEM) involves cutting a sample to a thickness comparable to the grain size, thus, creating structural relaxations that affect the grain boundary structure[4]. MD simulations, however, can be used to perform such analysis as specimens are 'virtual' and can be easily tailored to meet the specifications for the specimens used in an experiment. It should be noted that it is of utmost importance to produce nanostructures that are closely related to the specimens that are fabricated in an experiment.

Parallel supercomputers, like System X at Virginia Tech used in all the simulations in this research, can create samples of 3-dimensional (3D) grain boundary networks containing 100 grains with a 10 nm diameter, as shown in *Figure 1*, When using the periodic boundary conditions technique, the sample can be considered a small part of an infinitely large bulk nc sample. The construction of a 3D grain boundary network and subsequent simulation can be achieved in several ways: cluster assembly and compaction[5], rapidly quenching a melt containing pre-defined crystalline seeds[6], and a space-filling technique called the Voronoi construction[7, 8].

The application of large-scale MD simulations has provided new insight into plastic deformation of nanocrystalline metals. For most simulations, samples are placed

under uniaxial tension of a high load so that a measurable response can be obtained within time scales less than a nanosecond. In these early stages of deformation, information pertaining to grain boundary structure, dislocation emission from grain boundaries, and motions of a few atoms from boundaries can be obtained from MD simulations. However, because the time scale is so small compared to the hundreds of seconds in real experiments, simulations may not account for phenomena in later stages of deformation, and nor would they be able to observe effects due to long-range diffusion. Thus, MD simulations should not be regarded as absolute references to confirm nor disprove the presence of a deformation mechanism. However, they are still useful as qualitative models, especially when examining atomistic behavior, which is difficult to do with experiments. For example, in-situ analysis of deformation of nc-Ni with a time scale of several hundred picoseconds would pose a difficult task when considering an experiment. Such deformation, however, can be readily modeled using MD simulations.

Two approaches involving MD simulations are used to examine deformation: the first is applying a constant stress to the sample while observing the evolution of deformation over time, and the second is deformation by applying constant strain steps that are followed by a short relaxation time, simulating constant strain rate deformation, which is the method used in the present research[2].

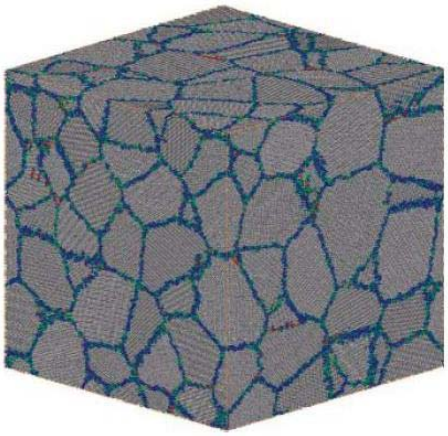

Figure 1: 3-D MD-simulated sample of nc-Ni with a mean grain diameter of 10 nm[8][1]

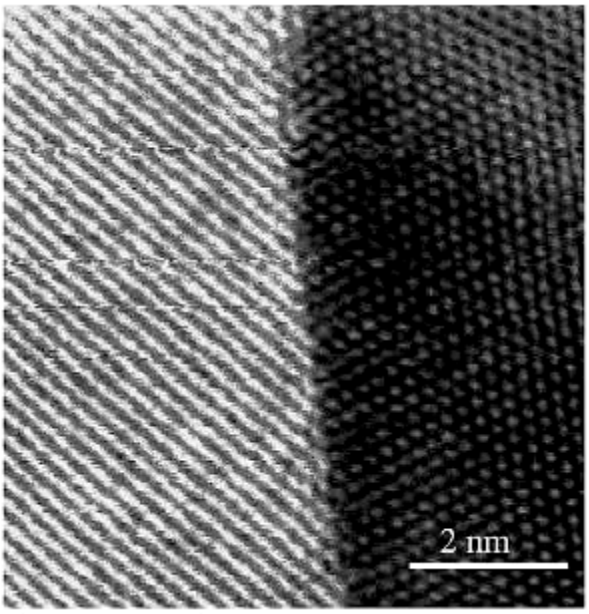

Figure 2: grain boundaries in electrodeposited nc-Ni[9][2]

1.4 Purpose

In this work two phenomena associated with nanocrystalline nickel (nc-Ni) are examined: stress effects and temperature effects on grain boundary migration in nc-Ni.

[1] *reprinted (abstracted/excerpted) with permission from Van Swygenhoven, Science, 2002. 296: p. 66-67. Copyright 2002. AAAS*

[2] *reprinted from Acta Materialia, 51, Kumar, Suresh, Chisholm, Horton, and Wang, Deformation of electrodeposited nanocrystalline nickel, 397-405, Copyright (2003), with permission from Elsevier*

As mentioned before, mechanical deformation and grain growth in nc metals are not clearly understood. With the availability of a powerful supercomputer, System X at Virginia Tech, MD simulations of tensile deformation and grain growth at various annealing temperatures were performed to examine stress and temperature effects on grain boundary migration, respectively.

Nanocrystalline nickel was chosen to be the subject of this analysis because various atomic potentials for nickel were available and because it is a face-centered-cubic (fcc) metal, which is a class of metal that has been the subject of many MD simulations. Also, nc-Ni has been experimentally synthesized in several studies. Thus, the results of the present work can be compared to other simulations to verify if identical phenomena have been observed, and to actual experiments to verify the experimental validity of the results.

If stress and temperature effects on grain boundary migration in nc-Ni have been elucidated, the results can translate to manipulating experimental synthesis techniques to produce desired grain boundary structures. These results have implications for processing of MEMS and NEMS, which require analysis of the deformation and growth behavior of their constituent materials to ensure their reliability in future applications.

2. Literature Review

2.1 Stress Effects on Grain Boundary Migration

Most bulk (average grain size > 100 nm) metals exhibit a flow stress profile described by the Hall-Petch relationship shown in Equation (2.0)

$$\sigma_y = \sigma_0 + K_y D^{-1/2} \tag{2.0}$$

where σ_y is the yield stress, D is the average grain size, and σ_0 and K_y are constants. As grain size decreases, dislocations pile up at grain boundaries, resulting in enhanced resistance to plastic deformation. It can be seen that refining the grain size from 100 nm to 10 nm, the metal exhibits a higher flow stress, but past the 10 nm limit, the mechanistic process changes, and the material weakens with decreasing grain size, as shown in *Figure 3*. Although there is a considerable amount of research that confirms this behavior by nanocrystalline metals, the actual deformation mechanism is not well understood. Several explanations from recent studies will be presented later in this section.

Shan and Mao[10] observed evidence of a deformation mechanism crossover of nc-Ni. Their results showed that the grain boundary controlled deformation increases rapidly with a scaling of D^{-4}. However, according to the Frank-Read dislocation multiplication model, D is inversely proportional to the nucleation stress within the material. Thus, it was concluded that there was a crossover regime as a result of competition between deformation controlled by nucleation and motion of dislocations and the deformation controlled by grain boundaries that were facilitated through grain boundary diffusion with decreasing D.

Van Swygenhoven et al[4] observed that in their MD simulations, at the smallest grain sizes all deformation is accounted for within the grain boundaries. Grain-boundary sliding was present at this regime and it was found that it was governed by individual jump events that each created minute amounts of strain. At larger grain sizes, dislocation activity was detected within grains and stacking faults were created by the motion of partial dislocations emitted and absorbed in opposite grain boundaries.

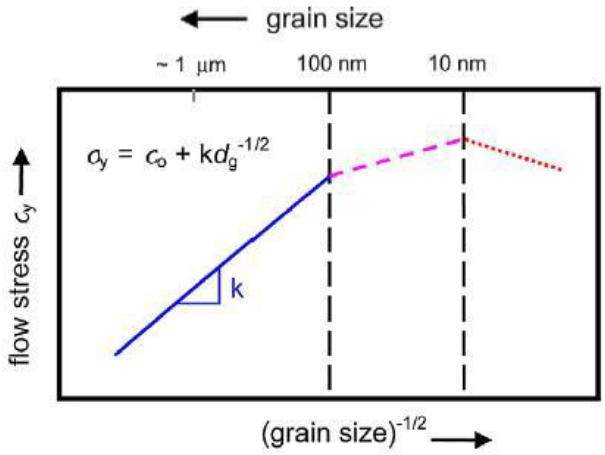

Figure 3: schematic of the Hall-Petch relation[2][3]

2.1.1 Deformation Behavior of Bulk Metals

Dislocation Models

There are several dislocation pile-up models for coarse-grained materials to explain the Hall-Petch relation. These models differ in the way that they account for grain boundaries as barriers to dislocations. One model suggests that grain boundaries restrict dislocation movement, resulting in concentrated stresses that facilitate dislocation sources in adjacent grains, activating slip from grain to grain. Another model suggests

[3] *reprinted from Acta Materialia, 51, Kumar, Van Swygenhoven, and Suresh, Mechanical behavior of nanocrystalline metals and alloys, 5743-5774, Copyright (2003), with permission from Elsevier*

that grain boundaries reduce the mean free path of dislocations which augments strain hardening[11].

Free Surfaces

Grain boundaries in the vicinity of free surfaces have a tendency to lie perpendicular to the surface, resulting in the reduction of its net curvature. Subsequently, the curvature becomes cylindrical as opposed to spherical and usually cylindrical surfaces move at slower rates than spherical surfaces with the same curvature. Another effect of a grain boundary terminating at a free surface is thermal grooving, when at high temperatures, grooves form on the surface where the grain boundaries terminate. Grooves play a major role in grain growth because they tend to anchor the ends of the grain boundaries (where they terminate), particularly the boundaries that are normal to the surface. To move itself from a groove, a boundary must increase its total surface area, and thus, its total surface energy. Thus, work is required to move the boundary, which implies that grooving restricts grain boundary movement. However, if the average grain size is small compared to the dimensions of the specimen, the thermal grooving effects are minimal[12].

Strain-Induced Migration

It is widely accepted that normal grain growth generally occurs due to strain energy stored in grain boundaries. However, crystals can also grow due to strain energy induced in the lattice via cold working. Strain-induced boundary migration differs from recrystallization because there is no formation of new crystals. Rather, boundaries in

between grains move in such a way that one grain will grow at the expense of the other. The crystalline region that is left behind during migration has a lower strain energy. Strain-induced boundary movement also differs from surface-tension-induced migration in that the boundary usually moves away from its center of curvature. An interesting aspect of strain-induced migration is that the boundary may actually increase its surface energy through the movement as opposed to lowering it. Strain-induced migration only occurs for relatively small to moderate amounts of cold working. A large amount of cold work will result in normal recrystallization[12].

2.1.2 Deformation Behavior of nc-Metals

As nc-metals contain a high density of grain boundaries, it is believed that their mechanistic behavior is governed by the behavior of the grain boundaries. Grain boundaries serve as sources and sinks for dislocations, and facilitate the reduction of stress within the material. It follows, then, that deformation mechanisms in nc-metals do not only depend on average grain size, like bulk materials, but are also affected by the grain size distribution as well as the grain boundary structure (low-angle versus high-angle grain boundaries).

It is the deformation characteristics of nanocrystalline metals that make them appealing for use in engineering applications. Such characteristics include ultra-high yield and fracture strengths, reduced elongation and toughness, superior wear resistance, and faster strain rates compared to the same metal at a microscale regime.

As mentioned before, the deformation mechanisms of nanocrystalline metals are not clearly understood. However, several recent studies have attempted to explain

mechanistic behavior of nc-metals using MD simulations. From many of these recent studies, it can be concluded that the deformation mechanisms are not largely dependent on dislocation movement, as in bulk metals, because dislocation sources are not expected to be present within grains at such sizes[2]. Instead, these studies propose a phenomenon that involves grain rotation and grain sliding. Conversely, there have been several recent studies that have concluded that indeed, the behavior of partial dislocations still govern deformation in nanocrystalline metals.

Rotational Deformation

Grain rotation induced by plastic deformation is a phenomenon that has been widely reported in many studies. However, the cause of grain rotation remains a topic of great debate. Some works report that rotational plastic deformation in nc-metals is thought to be primarily caused by dipoles of grain boundary disclinations, which are line defects that are classified by a rotation of a crystal lattice about its line. A disclination dipole is comprised of two dislocations that force rotation of a crystal lattice between them. These dipoles can only be energetically possible if the disinclinations are close to each other, as is the case in fine-grained nc metals. Motion of a disclination dipole along grain boundaries results in plastic flow along with rotation of the crystal lattice behind the disinclinations, as shown in *Figure 4*[13] .

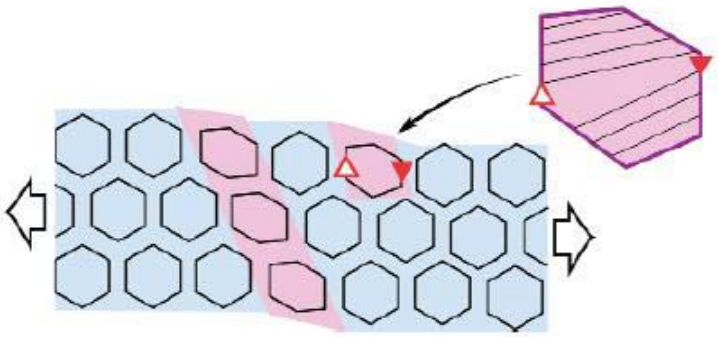

Figure 4: Motion of dipoles of disclinations (triangles) causes rotational deformation, as shown by the crystal lattice rotation behind them[13][4]

Murayama et al[14], used HRTEM analysis to examine rotational deformation in mechanically milled nc bcc-Fe. It was found that two partial wedge disclinations, or terminating tilt grain boundaries, could rotate a {110} plane between them by ~9°. Their work also indicated that the introduction of disclination defects into a metal during mechanical milling would increase the stored elastic energy within the material. Thus, disclinations were shown to possess the ability to cause deformation via rotation as well as strengthen a metal.

Shan et al.[15] performed in situ TEM analysis of nc-Ni films with an average grain size of ~ 10 nm. When the films were strained, changes in contrast over time were thought to be correlated with the rotation of grains. Not all grains exhibited a contrast change, indicating that rotation was not a global phenomenon within the samples. It was mentioned that several studies reported that the net torque on a grain was the driving force for rotation. This torque was thought to be caused by the misorientation dependence of energy of the grain boundaries that bound the grain from its adjacent grains. Furthermore, grain rotation was viewed as a sliding process along the periphery

[4] *reprinted (abstracted/excerpted) with permission from Ovid'ko, Science, 2002. 295: p.2386. Copyright 2002. AAAS*

of the grain and thus, changes in the grain shape were thought to be facilitated by diffusion, either through the grain boundaries or through the grain interiors. Dominance of grain boundary diffusion was considered a reasonable hypothesis provided that D was below a critical level at room temperature. If diffusion were truly dominant, then there would be a D^{-4} dependence on rotation rate. It was concluded that the grain rotation processes would decrease with time, as it was expected that over time, grains would find an orientation closer to equilibrium and reduce the overall energy of the system.

Chen and Yan[16] disagreed with the conclusion of Shan et al and formulated their own conclusions from the data. Quantitative measurements of relative displacements and grain sizes were made from the TEM micrographs. From these measurements, it was found that there were no systematic angle changes with time, indicating that plastic deformation did not occur in the films during loading. If, according to Shan et al., grains had truly rotated, then the surrounding grains would have had to exhibit a relative displacement, as plastic deformation cannot occur due to the rotation of a single grain. This was not the case, and Chen and Yan reasoned that the rotation Shan et al. observed was actually a result of grain growth and coalescence caused by electron-beam irradiation from the TEM and the applied stresses. Also, when examining a grain from Shan et al's study, they concluded that there was a linear relation between grain size and time that was consistent with a linear form of the classic grain growth equation, shown in Equation 2. Furthermore, the edge dislocations that Shan et al. observed, would be consistent with rotation growth theory reported in recent MD simulation studies, which will be discussed in the next section of this dissertation.

Shan et al.[17] suggested that Chen and Yan's analysis of the data was incorrect due to improper image contrast adjustments and misreadings of their original paper. Chen and Yan had implied that the data in Shan et al's paper exhibited linear grain growth by examining one grain. However, this assertion was refuted by Shan et al, as they claimed that the grains surrounding the single grain did not exhibit linear grain growth.

Grain-Boundary Sliding

Grain boundary sliding (GBS) plays a major role in creep and fine-structure superplasticity. A sliding occurrence involves of a few atoms moving from one position to another. These positions are both local minima in the total energy of the system. As the strain is increased, the system will prefer some minima to others and when the strain reaches a sufficiently high enough level, the system will move from one minimum to another. The system may require the energy from thermal vibrations to break through the last barrier. According to Schiotz[18], however, because MD simulations are performed over very small time scales, such a thermally activated process would only be sufficient when the thermal vibration energy is comparable to the barrier energy.

In another study conducted by Schiotz[19], it was suggested that as grain size decreased, a larger fraction of atoms would be present within the grain boundaries, making grain boundary sliding easier, resulting in the softening of the material. The decrease in flow stress in the Hall-Petch relation as *D* approached the smallest size, was attributed to grain boundary sliding.

Van Swygenhoven and Derlet[20] reported that grain-boundary sliding was accompanied by atomic shuffling. Such shuffling is a major component of grain-boundary sliding when a sample is undergoing tensile loading. It was believed that the shuffling was driven by the free volume present within the grain boundaries. Two types of shuffling were observed. One type was uncorrelated shuffling of individual atoms and the other was a correlated shuffling of a group of atoms. Hopping of grain-boundary was also observed, and was regarded as stress-assisted free-volume migration. This phenomenon, coupled with atomic shuffling, was reported to be the rate-controlling process of grain-boundary sliding.

Deformation Twinning

According to Hemker[21], deformation twins, which like all twins are Σ=3 grain boundaries, are created by partial dislocation motion, and are found in common fcc metals with low stacking fault energies and in fcc metals with high stacking fault energy when undergoing extreme deformation (

Figure ***5***). Controlled generation of twins and stacking faults could potentially create continuous grain-size strengthening and subsequently, increase strain hardening in fcc materials[22].

Embury et al.[23] formulated two conditions that had to be satisfied for deformation twins to be created within fcc metals. The first was that a change in the dominant slip condition must occur and second, a critical stress level must be achieved

locally at the twin site. Kumar et al.[9] reported that the critical resolved shear stress of the order of 300 MPa was required for deformation twinning to occur in Ni.

An analytical model based on classical dislocation theory was developed by Zhu et al.[24] to explain the nucleation and growth of deformation twins in nc-Al. It was observed that only a very high critical stress, achieved through high strain rates or low temperatures, was required to nucleate deformation twins, confirming Embury's postulate. Because of this high stress, they concluded that deformation twins could not be a major deformation mechanism in nc-Al. It was also reported that growth of deformation twins was achieved through the emission of partial dislocations on slip planes adjacent to the twin boundary.

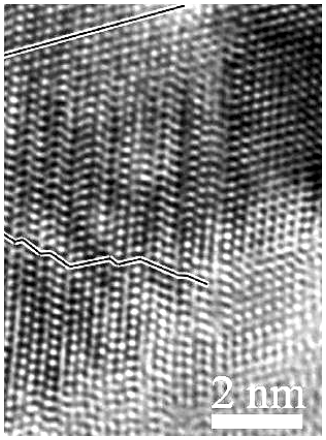

Figure 5: HRTEM image of deformation twins and stacking faults, both in the lower part of the grain.[25][5]

Growth Twins

Growth twins, also called annealing twins, are commonly found in fcc metals such as Ni (*Figure 6*) and Al. Such structures can be created from crystal nucleation and growth effects, as found in electrodeposited samples[9]. They can also be formed as a result of a harsh mechanical process such as ball milling and severe plastic deformation.

[5] *reprinted from Materials Science and Engineering A, Zhu and Langdon, Influence of grain size on deformation mechanisms: An extension to nanocrystalline materials, 234-242, Copyright (2005), with permission from Elsevier*

Few MD studies have been conducted on the effects of growth twins on plastic deformation and their interaction with emitted dislocations in nc metals. Most MD simulations do not contain growth twins in the starting microstructure, most likely because it is assumed that there are very few defects in $D < 20$ nm. While this may be true for some defects, the presence of defects, such as growth twins, have been reported in experimental studies with similar grain sizes[22, 26].

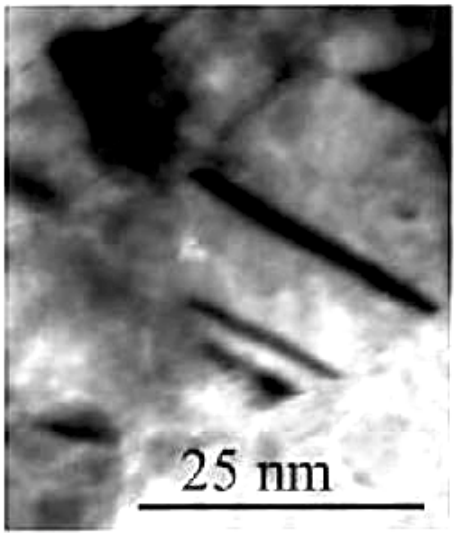

Figure 6: growth twin in electrodeposited nc-Ni[2]6

Van Swygenhoven et al.[27] were one of the few groups that ran MD simulations that included growth twins in the initial microstructure of their samples. To determine if twin boundary migration, in terms of generalized planar fault (GPF) energy, was the major deformation mechanism in nc-Cu, straining simulations of Cu samples containing growth twins were performed. In addition to the Cu, Ni samples were examined as well. The data pertaining to these two metals were compared to a previous study involving Al, so that a GPF comparison for several fcc metals could be obtained. It was reported that

[6] *reprinted from Acta Materialia, Kumar, Van Swygenhoven, and Suresh, Mechanical behavior of nanocrystalline metals and alloys, 5743-5774, Copyright (2003), with permission from Elsevier*

growth twins could potentially change the deformation mechanism in fcc metals, but the extent to which they affected the mechanism varied amongst the metals. Cu and Ni exhibited twin migration energies similar to their partial dislocation energy barriers, which was not the case in the study of Al.

Growth twins influence the plasticity of the metal via twin migration, which in fcc metals, is the motion of an existing twin plane to an adjacent (111) plane through partial dislocation slip at the associated (111) plane. Partial dislocation slip is correlated to the GPF energy curve[28] .

Free Surface Effects

Van Swygenhoven and Derlet[4] investigated the effects of the presence of two parallel free surfaces on grain-boundary dynamics of nc-Ni through MD simulations. Two effects were examined: the influence of the relaxation process resulting from the creation of the two surfaces on grain morphology, and the deformation behavior of the samples under unixaxial stress. Two types of samples were examined: a sample that did not contain free surfaces and was considered periodic (and thus, could be replicated to describe a bulk material) and a sample with free surfaces. It was observed that there was additional plastic strain and an increase in strain rate in the surface sample compared to the periodic sample. These effects were attributed to, depending on *D*, increased dislocation activity and increase in grain-boundary sliding. Grain-boundary sliding was enhanced due to the presence of the surface. Also, in both the surface and non-surface samples, the average sliding vector was parallel to the grain boundary. However, in the

surface sample, there was a perpendicular component to the surface, resulting in increased surface roughness.

It was also observed that deformation from the uniaxial stress led to an increase in triple-junction migration and growth. The volume of triple-junctions was high where they intersected the surfaces. As D, increased, it was expected that the triple-junction effects would decrease. Atomic shuffling occurred in areas where there was excess free volume or crystallographic mismatches. Despite the atomic shuffling, no significant change in the grain boundary structure was reported.

The conclusions of the experiment were that the effects of the parallel surfaces were felt throughout the sample for sample thickness on the order of $2D$, that increasing grain size leads to increased dislocation activity, and defects that terminated at the surface acted as dislocation emitters. If the sample thickness were several orders higher than $2D$, it would not be expected for the surfaces to have a large influence on the deformation within the material.

Grain Growth Through Deformation-Induced Grain Rotation-Coalescence

Jin, et al[29], performed nanoindentation experiments on sub-micron and nc-Al films at room temperature and observed two similar deformation responses, respectively. In the sub-micron Al film, though dislocation activity was still present, the deformation mechanism of deformation-induced grain growth was also present. During the initial stages of indenting a grain boundary, elastic deformation was followed by dislocation nucleation and extensive dislocation multiplication (as predicted by the Frank-Read model). Subsequently, the boundary between the two grains moved across the smaller

grain and vanished, resulting in the coalescence of the adjacent grains into a single, larger grain, as depicted in *Figure 7*. Similar phenomena were observed in the nc-Al film, but an important distinction is that according to TEM analysis, grain rotation occurred in addition to the grain growth in the nc-Al film immediately following indentation.

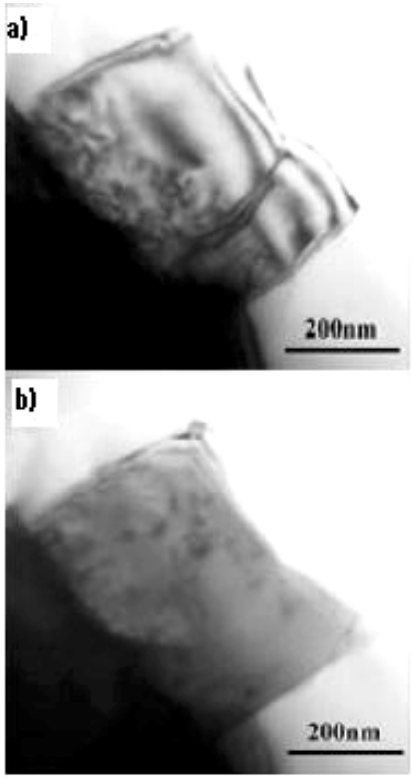

Figure 7: a) bright-field image of adjacent grains before indentation b) bright-field image of a larger single grain after indentation[29]*[7]*

[7] *reprinted from Acta Materialia, Jin, Minor, Stach, and Morris, Direct observation of deformation-induced grain growth during the nanoindentation of ultrafine-grained Al at room temperature, 5381-5387, Copyright (2004), with permission from Elsevier*

2.2 Thermal Effects on Grain Boundary Motion

2.2.1 Thermal Effects in Bulk Metals

Experiments have shown that after a metal has been plastically deformed (through cold work, for example), it can be heat-treated to revert the properties and structure of the metal back to their pre-stressed states. This restoration is caused by two processes that occur at elevated temperatures, recovery and recrystallization. Sometimes these processes are followed by a third high-temperature process, grain growth. However, grain growth does not require a metal to under recovery and recrystallization to occur.

Grain boundaries of metals contain energy, which is termed grain boundary energy. As grains increase in size, the total grain boundary area decreases, resulting in the reduction of the total energy of the metal, which drives the grain growth process. Grain growth is facilitated through the motion of grain boundaries. Not all grains will increase in size, as some grains will grow at the expense of smaller grains that vanish. It is expected that the average grain size will increase with time, and for most growth processes, there will be a distribution of grain sizes. Grain boundary motion is essentially short-range diffusion of atoms across a boundary. Atomic motion moves in the opposite direction of grain boundary motion[30].

Grain growth in polycrystalline materials, such as metals and ceramics, usually follows the classical growth law, as shown in Equation (2.2)

$$D^n - D_0^n = Kt \tag{2.2}$$

where D is the mean diameter of a grain, D_0 is the initial grain diameter, K and n are constants that are independent of time, and t is time.

Many times, metals exhibit normal grain growth, which is characterized by uniform grain structure in which the distribution of size and shape remains the same throughout the specimen while the average grain size increases[31]. In this case, the growth law takes the form of Equation (2.3)

$$D^2 - D_0^2 = Kt \tag{2.3}$$

where $n = 2$. If the initial grain size, D_0, is assumed to be very small, it can be neglected,and the grain growth law can be manipulated to exhibit the form shown in Equation (2.4)

$$D = Kt^{1/2} \tag{2.4}$$

Because t is raised to the power of ½, it is implied that the grain growth process is a parabolic or diffusion-controlled process.

2.2.2 Thermal Effects in nc Metals

Excess Volume

Grain boundaries in a material of a polycrystalline state contain excess energy compared to those in a single-crystalline state. Thus, there is a thermodynamic driving force that reduces this excess energy via reduction of grain-boundary area or through an increase in average grain size, D According to classical models of grain growth, factors such as the intrinsic grain-boundary mobility which is temperature-dependent, defect concentrations, second-phase precipitates, and segregation of impurity atoms, control the

growth rate of D. Because all these factors are independent of D, classical models assume that a single growth mechanism controls the growth rate at all length scales.

This assumption has been proven true for $D > 1$ μm. However, in nanocrystalline materials, where $D < 100$ nm, the growth rate is much slower than in the microscale regime, and thus, most likely is not controlled by the same factors in the microscale regime. Several studies have deduced that the cause of this phenomenon is the solute drag resulting from the presence of impurities during the synthesis of nanocrystalline materials.

A recent study indicated that growth in the nano-regime may not deal with any of the previously mentioned factors. Instead, it has been postulated that there exists a grain size, D_C, under which the growth mechanism is not boundary-curvature-driven diffusion, but rather grain-boundary migration and the motion of grain-boundary features such as triple junctions, or the excess volume localized in the core regions of grain boundaries. All of these postulates state that D has a linear time-dependency for $D < D_C$, as opposed to the $t^{1/2}$ dependency found in coarser regimes[3].

Excess volume in a polycrystalline material is present within grain boundaries because grain boundaries are less dense than their neighboring crystalline grains. At sufficiently small grain sizes, it has been shown that grain-boundary migration rate is controlled by the transport of excess volume. When the total grain-boundary area is reduced during grain growth, the excess volume within the annihilated boundary must be transported elsewhere in the sample or transported to the surface. In the beginning stages of grain growth, it has been shown that excess volume is transported within the material in the form of vacancies, which creates a nonequilibrium state. This nonequilibrium

concentration of vacancies increases the Gibbs free energy, which works against the decrease in free energy due to grain-boundary area reduction. When $D < D_C$, the reduction in the overall driving force due to the vacancies results in severe attenuation of growth kinetics, which subsequently results in a linear growth profile for D. Once D is greater than D_C, production of excess vacancies no longer governs the growth rate and growth kinetics exhibit the classical parabolic growth profile[32].

Grain Growth Through Thermally-Induced Grain Rotation-Coalescence

Another potential growth mechanism in nanocrystalline materials is grain-rotation-induced-coalescence. This process involves neighboring grains to coordinate their rotations in such a way as to remove their common grain boundary, resulting in the coalescence of the grains. Grain coalescence will reduce the overall energy of the grain boundary work and as a consequence, rotation can only proceed if grain boundary energy is anisotropic.

The grain boundary energy is determined by the angle of misorientation between neighboring grains. When one grain changes its orientation via rotation, the grain boundaries shared with neighboring grains will change in orientation as well, leading to the reduction of the total energy of the these grain boundaries. When neighboring grains achieve the same orientation, they coalesce and form a single, larger grain. As a result of coalescence, the number of grains in the system decrease discontinuously as grains combine to form a larger grain[33].

Phillpot, et al.[34] have developed a model that combines grain rotation-coalescence with curvature-driven grain boundary migration. In this model, grain-rotation leads to

coalescence, resulting in the annihilation of a shared grain boundary and the removal of two triple junctions. This in turn results in two highly-curved curved, and thus, highly unstable, grain boundaries, which will induce rapid grain growth through grain boundary migration.

Triple-Junction Drag Effects

Nanocrystalline materials not only contain a high density of grain boundaries but also a high density of triple junctions as well. In many computer simulations, it is implied that triple junctions do not affect grain boundary migration and that their only purpose in grain growth is to maintain the thermodynamically dictated equilibrium angles where grain boundaries meet. This assumption is found in the Von Neumann-Mullins relation, which defines the rate of change of grain area during grain growth. This relation can be seen in Equation (2.5)

$$\frac{dS}{dt} = \frac{-A_b \pi}{3}(n-6) \tag{2.5}$$

where S is the grain area, A_b is the grain boundary area, and n is the number of triple junctions for each grain and defines the topological class of the grain.
The three tenets of the Von Neumann-Mullins relation are as follows:

1. all grain boundaries have the same mobility (m_b) and surface tension (γ) which are independent of misorientation and the crystallographic orientations of the grain boundaries
2. the mobility of a grain boundary is independent of the grain boundary velocity

3. triple junctions do not affect grain boundary motion and the contact angles at triple junctions are always at an equilibrium angle of 120°

The first tenet in the Von Neumann-Mullins relation is confirmed by the uniform boundary model while the second tenet is confirmed by absolute reaction rate theory. It is the third tenet that requires confirmation via experiments.

shows a grain surrounded by other grains and the resulting triple junctions. Gottstein and Shvindlerman[1, 35, 36] have shown that the vertex angle θ can deviate from the equilibrium angle for a triple junction when a low mobility of the triple junction stymies grain boundary migration. This effect depends on temperature; as the temperature increases, the triple junctions have less of an effect on grain boundary migration. Their experiments verified that there exists a transition from triple junction kinetics to grain boundary kinetics and that triple junctions exhibited a finite mobility. This transition does not only depend on grain boundary and triple junction mobility, but on grain size as well. When grain growth kinetics are controlled by triple junctions, it was found that the initial stage of growth was linear. The drag due to triple junctions resulted in an "increase" of shrinking grains and a "decrease" of growing grains. Their experiments also demonstrated that there is no linear relationship between growth rate and the number of sides. Thus, the third tenet of the Von Neumann-Mullins relation is not necessarily true at the nanoscale regime, where it has been shown that triple junctions can affect grain boundary motion.

Experiments by Novikov[37] agreed with Gottstein and Shvindlerman's work. It was observed that low mobility of triple junctions could influence the evolution of 2D microstructure during grain growth in three ways. The first is inhibiting grain growth, the

second is the occurrence of a linear growth profile in the initial stage of grain growth, and third, the temporal increase of grain size nonhomogeneity.

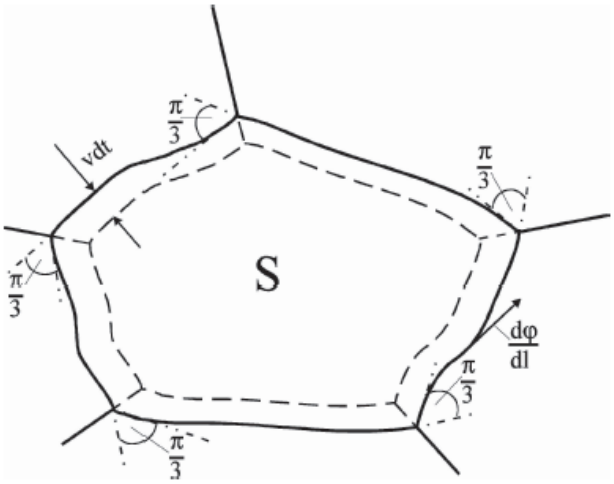

Figure 8: grain bordered on each side by an adjacent grain, resulting in triple junctions[8]

Deformation Effects from Annealing

Annealing has traditionally been viewed as a process that could strengthen a metal. Low temperature annealing effects on the strength of electrodeposited nc Ni were examined by Wang et al[38]. It was found that at annealing temperatures ≤ 150°C, the Ni increased in yield stress and in ultimate tensile strength while there was no apparent reduction in the elongation failure. Such behavior had not been reported before for electrodeposited nc metal.

Simulations performed by Van Swygenhoven et al.[39] were used to compare the deformation response of annealed nc-Ni with as-prepared nc-Ni. Annealed nc Ni was observed to have grain boundaries and triple junctions closer to an equilibrium configuration, and displayed reduced plasticity (or increased strength), indicating that

[8] *Journal of Materials Science, 40, 2005, 829, Special Section: Grain Boundary and Interface Engineering, Gottstein and Shvindlerman, Figure 5, Copyright 2005 Springer Science + Business Media, Inc., with kind permission of Springer Science and Business Media*

relaxing the structure can produce beneficial effects. Strain rate measurements on the two types of samples yielded similar results, suggesting that the samples exhibited similar atomic processes. Also, changes in grain boundaries during both mechanical and thermal loading were attributed to atomic shuffling and diffusion, or stress-related diffusion.

3. Simulation Methods and Analysis Techniques

The most rudimentary atomistic model of a metal is an array of atoms interconnected with springs. More elaborate techniques have been developed that replicate material properties to improve simulations as accurate representations of experimental phenomena. One such technique is the embedded atom method (EAM), which was used in all the simulations present within this study[40, 41].

3.1 Molecular Dynamics (MD) Simulations

Quantum mechanics, through the time-dependent Schrodinger equation, would provide the most accurate representation of atomic motion. However, the calculations involved in such a method would be complex and cumbersome, and the results would be difficult to apply to the motion behavior of the atoms. It has been found that a classical mechanics approach, though not as accurate as a quantum mechanics approach, can provide a sufficiently accurate representation of atomic motion. MD simulations, which are based on classical mechanics, can be used to compute the equilibrium and transport of various particle systems by solving the equations of motion for each component.

3.1.1 Equations of Motion

The classic Hamiltonian, H, is regarded as the sum of the kinetic and potential energies or simply the total energy of the system. A system of N point masses is expressed using the Hamiltonian as

$$H(\rho_i, r_i) = \sum_{i=1}^{N} \frac{1}{2m_i} p_i^2 + U(r_i) \tag{3.1}$$

where p_i is the momentum of particle i where $p_i = m_i(dr_i/dt)$ where r_i is the position vector of particle i, m_i is the mass, and U is its effective potential. In an isolated system, the

Hamiltonian is a constant, E, as shown in Equation (3.2)

$$H(\rho_i, r_i) = \sum_{i=1}^{N} \frac{1}{2m_i} p_i^2 + U(r_i) = E \tag{3.2}$$

Using the total Hamiltonian shown in Equation and the isolated form in Equation , it is possible to derive equations of motion for the particles of the system shown in Equations

$$\dot{p}_i = \frac{\partial H}{dr_i} = \frac{\partial U}{\partial r_i} = f_i \tag{3.3}$$

$$\dot{r} = \frac{\partial H}{\partial p_i} = \frac{p_i}{m_i} \tag{3.4}$$

where f_i is the force applied to particle i. Equations 3.3 and 3.4 can be used to yield Newton's second law:

$$m_i \ddot{r}_i = f_i \tag{3.4}$$

Thus, it can be seen that equations of motion are integrated through a numerical method to govern MD simulations. The atomistic system of an MD simulation will evolve over time as particle motion in phase space is governed by the equations of motion.

3.1.2 The Embedded Atom Method (EAM)

Interactions amongst atoms within an MD system are governed by interatomic potentials. These potentials are created to replicate experimental data as closely as possible, to provide practical information concerning atomistic behavior. Potentials involve empirical formulas that simulate material characteristics such as the heat of solution, lattice constants, and surface energies. A well-known technique used to simulate atomic interactions is the Embedded Atom Method (EAM), which was developed by Dawes and Burkes, and is currently used to mimic experimental interactions amongst atoms in metals and intermetallic compounds.

In this work, two atomic potentials were used to govern atomic interactions in the studies. The main potential, which was used in both the stress effects and temperature effects components of this study, is the Voter, or standard, potential, created by Voter and Chen[42]. The alternate potential, created by Mishin and Farkas[43], was used only in the stress effects components of the study.

The total energy of a monoatomic system is written as

$$E_{total} = \frac{1}{2}\sum_{ij} V\left(r_{ij}\right) + \sum_{i} F\left(\overline{\rho}_i\right) \tag{3.5}$$

where $V(r_{ij})$ is a pair potential as a function of the tensor r_{ij}, which s the distance between atoms i and j. F is the embedding energy that is a function of the host density, $\overline{\rho}_i$ applied at site i by all of the other atoms within the system. The host density is given by

$$\overline{\rho}_i = \sum_{i \neq j} \rho\left(r_{ij}\right) \tag{3.6}$$

The EAM potential information for nickel is shown in *Table 1,* which is based on data from Mishin and Farkas[43]:

Table 1: EAM potential data for nickel[9]

	Experiment or *ab initio*	Present work	Voter and Chen (Ref. 9)
Lattice properties:			
a_0 (Å)*	3.52[a]	3.52	3.52
E_0 (eV/atom)*	−4.45[b]	−4.45	−4.45
B (10^{11} Pa)*	1.81[c]	1.81	1.81
c_{11} (10^{11} Pa)*	2.47[c]	2.47	2.44
c_{12} (10^{11} Pa)*	1.47[c]	1.48	1.49
c_{44} (10^{11} Pa)*	1.25[c]	1.25	1.26
Phonon frequencies:			
$\nu_L(X)$ (THz)†	8.55[d]	8.71	10.03
$\nu_T(X)$ (THz)†	6.27[d]	6.38	6.68
$\nu_L(L)$ (THz)	8.88[d]	8.53	10.04
$\nu_T(L)$ (THz)	4.24[d]	4.31	4.37
$\nu_L(K)$ (THz)	7.30[d]	6.98	8.08
$\nu_{T_1}(K)$ (THz)	5.78[d]	5.68	6.04
$\nu_{T_2}(K)$ (THz)	7.93[d]	8.04	9.23
Other structures:			
E(hcp) (eV/atom)*	−4.42[e]	−4.43	−4.44
E(bcc) (eV/atom)*	−4.30[e]	−4.30	−4.35
E(diamond) (eV/atom)†	−2.51[e]	−2.50	−2.61
Vacancy:			
E_v^f (eV)*	1.60[f]	1.60	1.56
E_v^m (eV)*	1.30[f]	1.29	0.98
Interstitial:			
E_I^f (O_h) (eV)		5.86	4.91
E_I^f ([111]-dumbbell) (eV)		5.23	5.37
E_I^f ([110]-dumbbell) (eV)		5.80	5.03
E_I^f ([100]-dumbbell) (eV)		4.91	4.64
Planar defects:			
γ_{SF} (mJ/m^2)*	125[g]	125	58
γ_{us} (mJ/m^2)		366	225
γ_T (mJ/m^2)	43[g]	63	30
γ_{gb}(210) (mJ/m^2)		1572	1282
γ_{gb}(310) (mJ/m^2)		1469	1222
Surfaces:			
γ_s(110) (mJ/m^2)†	2280[h]	2049	1977
γ_s(100) (mJ/m^2)†	2280[h]	1878	1754
γ_s(111) (mJ/m^2)†	2280[h]	1629	1621

The EAM functions for the interactions of nickel atoms are plotted in *Figure 9*.

[9] *reprinted Table II with permission from Mishin and Farkas, Physical Review B, 59, 3393, 1999. Copyright (1999) by the American Physical Society.*

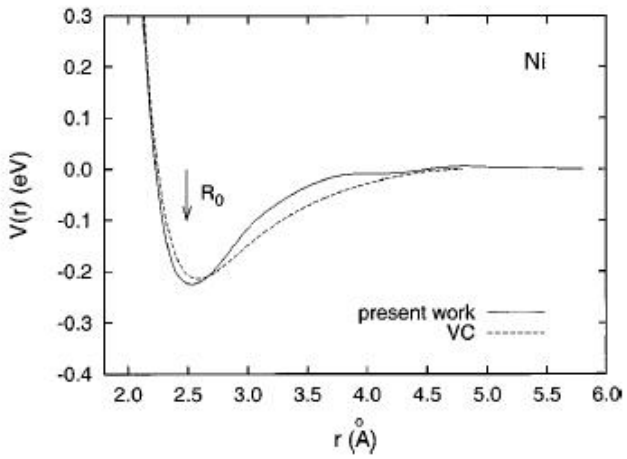

Figure 9: EAM functions for nickel, plotted potential energy (ev) vs. distance (angstroms)[43][10]

The simulations were run in LAMMPS[44], and the results were analyzed using Ras-Top[45] and Amira[46] visualization programs.

3.1.3 The Molecular Dynamics Method

Before a standard MD simulation is executed, system characteristics such as number of and type of atoms, atomic mass, and atomic interactions are defined. Then the initial configuration, of the system, at $t = 0$, is inputted. This configuration entails the initial positions, which are dictated by the crystallographic properties of the materials, and initial velocities, established as functions of initial temperature. Velocities are obtained from the temperature function using a statistical mechanics approach, such as a Maxwell-Boltzmann distribution. The time step, Δt, the integration variable in this case, must be assigned a value that is both small compared to the highest frequency motion to provide accurate integration over all motions, and large as possible so that the simulation

[10] *reprinted Figure 1b with permission from Mishin and Farkas, Physical Review B, 59, 3393, 1999. Copyright (1999) by the American Physical Society.*

has enough time to provide accurate results. Initial force calculations are followed by iterative force and velocity calculations for $t = t + \Delta t$.

After initial atomic interactions are computed, the specimen evolves while being constrained by the equations of motion, until the specimen's properties have reached a steady-state condition. Once the atomic potential has been configured, the MD simulation proceeds and allows the forces to act on the atoms as they migrate. These forces include such phenomena as diffusion effects, deformation effects, and temperature effects. The output of the simulation can be examined to elicit the causations and correlations of the constituent phenomena.

3.2 Stress Effects on Grain Boundary Motion

In the stress effects component of the study, the specimen was a 5 nm^3 block of nc-Ni that initially contained 15 grains, and was analyzed in two forms, one with free surfaces, and one without free surfaces (periodic, as they could be replicated to simulate bulk material), throughout the tensile deformation process. This was done to examine the effects of free surfaces on grain boundary migration during the deformation. The tensile deformation was a constant strain rate process that proceeded until the sample was elongated by 15% in the span of 450 ps. The atomic potential of the specimens in both surface and non-surface form, were governed by Voter and Yuri (standard and alternate, respectively) potentials, to ensure that the results were due to grain boundary behavior and not due to the governing potential. Grain boundary motion, as a function of grain boundary displacement versus deformation time, grain rotation, and grain sliding were examined during this process.

3.3 Thermal Growth and Grain Boundary Motion

In the temperature effects component of the study, a specimen identical to the one that underwent tensile deformation was used. All the thermal specimens were periodic and thus, did not contain free surfaces. Grain boundary motion was examined at the following annealing temperatures: 900, 1000, 1100, 1200, 1300, and 1450 K. The annealing times were 900, 300, 150, 150, 150, and 150 ps, respectively. Grain boundary motion, as a function of grain boundary displacement versus annealing time, was examined, as was average grain boundary energy per atom, average grain size, and grain rotation.

3.4 Grain Boundary Motion Analysis

Grain boundaries that moved parallel to themselves throughout the stress or grain growth process were examined in this study. Parallel boundaries were chosen so that grain boundary rotation would not have to be taken into account. As all the examined grain boundaries were straight, the two endpoints of the grain boundary were tracked for each timestep. The displacement between timesteps was calculated using the distance formula for the two endpoints, and averaging the summed distances of the endpoints at each timestep. Subsequent displacements were added on to obtain the absolute displacement over time. This calculation can be seen in Equation (3.7).

$$L = 0.5 \times \left[\sqrt{\left(a_1 - a_1^{'}\right)^2 + \left(a_2 - a_2^{'}\right)^2} + \sqrt{\left(b_1 - b_1^{'}\right)^2 + \left(b_2 - b_2^{'}\right)^2} \right] \qquad (3.7)$$

where L is the displacement in the current timestep, (a_1', a_2') and (a_1, a_2) are the previous and current first endpoint, respectively, and (b_1', b_2') and (b_1, b_2) are the previous and current second endpoint, respectively. This calculation can be further elucidated by the schematic shown in *Figure 10*. After each time step, grain boundary displacement was added on to the displacement in the prior timestep. Grain boundary displacement was plotted against timestep, resulting in linear plots, and the slopes were used as velocities of the grain boundary.

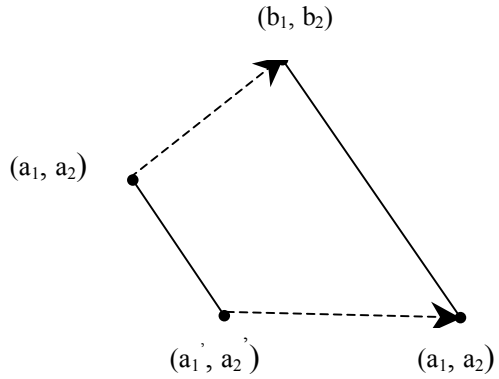

Figure 10: schematic of moving grain boundary (a) in initial position 1 and (b) final position 2

3.5 Energy Calculations

The energy relationship involving the total specimen energy, E_T, grain size, D, grain boundary area, $A(t)$, perfect crystal energy E_{PC}, and the grain boundary energy, $\gamma_{GB}(t)$, of the specimen are shown in Equation (3.8). It should be noted that both grain boundary area, A, and γ_{GB} are both functions of time, t.

$$E_T = E_{PC} - A(t)\gamma_{GB}(t) \tag{3.8}$$

The number of grains within a sample, N, is equal to the ratio of the volume of the entire specimen, V, to the volume of an average grain with a cube geometry, D^3, as illustrated in Equation (3.9)

$$N = \frac{V}{D^3} \tag{3.9}$$

The surface area of a grain with a cube geometry is $6D^2$, and thus, it follows that the surface area for N grains is $6ND^2$, and assuming that they are adjacent grains, the surface area is $3ND^2$. The grain boundary area, A, is shown in Equation (3.10)

$$A = 3ND^2 \tag{3.10}$$

Substituting Equation (3.9) in for N in Equation (3.10) gives Equation (3.11). The following result is also valid for spherical grain geometry.

$$A = \frac{3V}{D} = \frac{3V}{D(t)} \tag{3.11}$$

It can be seen from Equation (3.11) that grain boundary area is inversely proportional average grain size, D, and is thus, inversely proportional to the square root of the time step, for normal growth, shown in Equation (3.12)

$$A \ \alpha \ \frac{1}{\sqrt{t}} \tag{3.12}$$

As total specimen energy, E_T, is proportional to A, it follows that

$$E_T \ \alpha \ \frac{1}{\sqrt{t}} \tag{3.13}$$

Equation (3.13) is also assuming normal grain growth. The energy per atom, *K*, was also obtained using Equation (3.8).

3.6 Mobility Calculation

Grain boundary mobility is calculated using Equation (3.14)[56]

$$v = MF \qquad (3.14)$$

where *v* is grain boundary velocity, *M* is mobility, and *F* is the driving force, which in this case is assumed to be the curvature of the grain boundary, $2\gamma_{GB}(t)/D(t)$. At 1300 K at 25 ps (sufficient time for the microstructure to achieve equilibrium), the grain boundary mobility is 84.912 $m^4/s \cdot J$.

3.7 Grain Rotation

To measure grain rotation with respect to time, the center grain was examined in both the stressed and annealed specimens. This is because the center grain is automatically grown along the [100] axis and thus, following its atoms would be relatively simple as there is an initial reference that is easy to locate. A line of atoms was followed throughout the stress or annealing process. Only atoms that rotated in one rotational axis were measured, as it would have been difficult to track atoms that rotated in two or three rotational axes. A line of atoms is tracked in a stressed sample, shown in *Figure 11*. Only one grain could be examined due to time constraints.

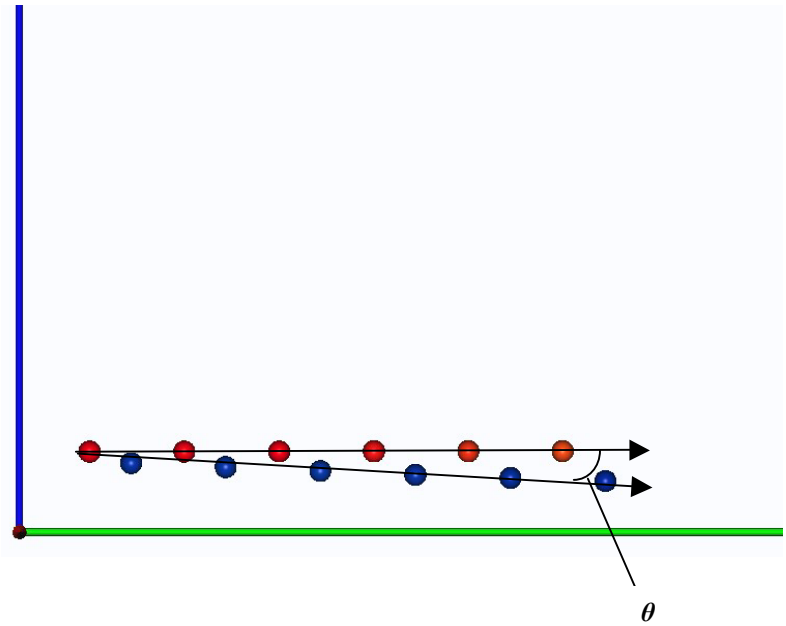

Figure 11: rotation of atoms in a sample grain (a) from an initial state (red) to a (b) final configuration after 450 ps (blue)

3.8 Average Grain Size Analysis

To obtain average grain sizes for the annealed samples, an intersection method was used. Essentially, at every timestep, 10 evenly spaced lines were drawn across the 2-D RasTop image. The number of times a line intersected a grain boundary was recorded and added on to the total number of intersections for a specimen at every timestep. A schematic of this process is shown in *Figure 12*, where some intersections have been circled.

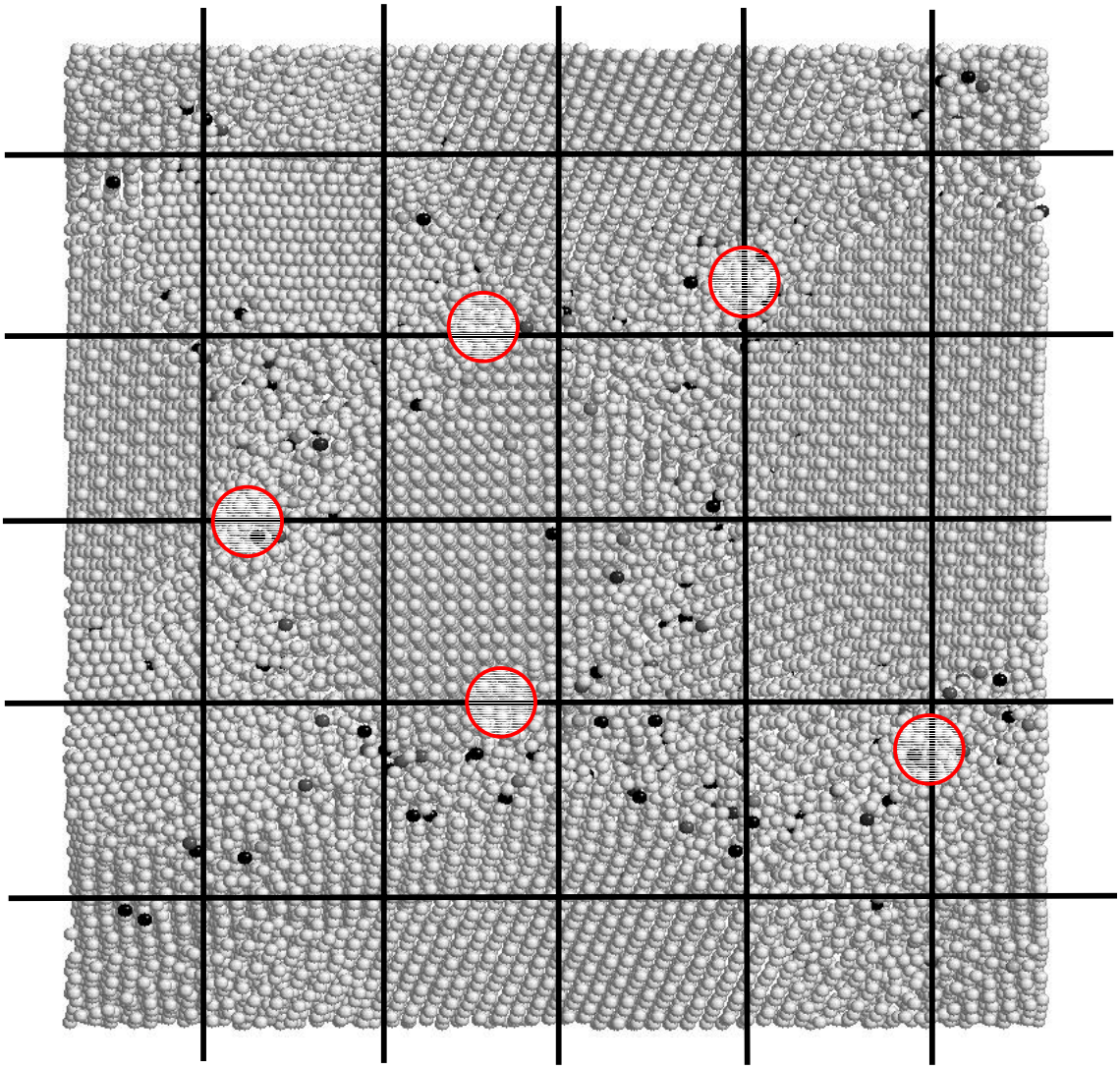

Figure 12: schematic of intersection method used to obtain average grain size; sample instances of intersections are circled

4. Results/Discussion

4.1 Tensile Stress Effects on Grain Boundary Motion

4.1.1 Results/Discussion

Very few dislocations can be observed within both the non-surface and surface samples after deformation, indicating that the deformation mechanism during a tensile stressing procedure is most likely not dislocation-driven, and instead, is most probably related to grain rotation or grain-boundary sliding, as was concluded by Van Swygenhoven and Derlet[4]. Budrovic, et al.[47] confirm the lack of dislocation debris and absence of work hardening in nc-Ni using electrodeposited nc-Ni and MD simulations. The lack of dislocations present in both the surface and non-surface samples is not surprising. At bulk length scales where D is in the range of 30 nm – 100 nm, dislocation-mediated plasticity is the dominating deformation mechanism[10]. However, in fine-grained metals, where $D < 10$ nm, as is the case with our specimens, the length scale is expected to be too small for dislocation sources to be able to function, which agrees with the 'reverse Hall-Petch' relation. Furthermore, unlike bulk metals, there have not been any reports of the presence of dislocation pile-ups. Also, it is widely accepted that if dislocations are present within specimens of $D < 10$ nm, they will be emitted and absorbed at the grain boundaries, which serve as very effective dislocation sinks and sources[2].

Recent MD studies have reported that nc-metals relieve applied stress through grain boundary sliding and the generation of partial dislocations that sweep across the

grain and are absorbed into the opposing grain boundary. The presence of partial dislocations within the specimens has been confirmed by the presence of stacking faults and twins, which are created by partial dislocations[21]. In our specimens, however, neither stacking faults nor twins (due to deformation or growth) are observed, implying that partial dislocations may be absent. However, the presence of free surfaces would imply that part of the deformation mechanism, at least in the surface samples, is grain boundary sliding. Several studies[2, 10, 15, 18, 20, 21] have reported that the grain boundary network facilitates grain boundary sliding through various mechanisms such as interface and triple junction migration, dislocation activity within the boundary itself, and grain rotation, which is also observed in the specimens.

Free surfaces effects on grain boundary motion driven by a tensile stress can be seen in *Figure 13*. The initial grain structure is shown in *Figure 13(a)* and the final grain structures are shown in the non-surface case and surface case in *Figure 13(b)* and *(c),* respectively. Notice that the free surfaces are aligned along the tensile axis. It can be seen in both samples that some grains have grown while some others have disappeared, confirming grain growth phenomena where grains grow at the expense of others. Grain growth due to an imposed stress is expected, as shown in many recent studies. However, the theories of stress-mediated growth vary. Clark and Alden[48] proposed that grain boundary sliding caused by the stress increases the vacancy concentration within and adjacent to grain boundaries, facilitating grain boundary diffusion, which in turn, leads to grain growth. Friedez et al[49] constructed a model that suggested grain growth is enhanced by stress through the reduction of the activation energy of grain boundary migration. A recent MD study conducted by Wolf, et al[50] indicated that the mechanism

for grain growth was grain boundary sliding, which may also be the mechanism of grain growth in this present work.

In the surface case in *Figure 13(c)*, slight necking occurs along the free surfaces. Shearing planes are present within both specimens, as shown by the arrows. According to a study conducted by Van Swygenhoven, et al.[51], it is suggested that shear planes are the result of a cooperative plastic deformation process involving grain-boundary migration through grain-boundary sliding, grain-boundary migration through intragranular slip, and grain rotation. It is also mentioned that grain boundary sliding becomes a major plastic deformation process when $D \sim 5$ nm, which is on the order of the grain sizes found in the specimens in this study.

A difference in deformation behavior between non-surface and surface specimens can be seen in the stress-strain curve shown in *Figure 14*. Inspection of *Figure 14* reveals that for both potentials, the surface samples require less yield stress to achieve the same elongation as their non-surface counterparts, indicating that they are more easily deformed via tensile loading. This is most likely attributed to the presence of the free surfaces facilitating grain boundary sliding, as will be explained below.

Because the surface samples exhibit a lower yield stress than the non-surface samples, it would seem intuitive that they would exhibit higher grain boundary velocities, as well. However, this does not appear to be the case, as illustrated in *Figure 15*, which is a plot of grain boundary displacement vs. time for a sample grain boundary found in both the surface and non-surface samples at the standard potential. The grain displacement has a linear relationship with time, and thus, it follows that the slope of the plot is the grain boundary velocity. It can be seen that the slope, and thus, the grain

boundary velocity, is higher in the non-surface case. This does not appear to be an isolated case, as the data collected in this study confirm that surface samples did indeed exhibit lower average grain boundary velocities. *Figure 16* shows the distribution of the grain boundary velocities for both the surface and non-surface samples at the standard potential. Note that the peak of the distribution of the grain boundary velocities for the surface case is at a lower velocity value (3 m/s as opposed to 4 m/s) than for the non-surface case. The average grain boundary velocities (and associated standard deviations) for the surface and non-surface cases are shown in *Table 2*.

The lower yield stress and average grain boundary velocity exhibited by the surface specimen is most likely attributed to grain boundary sliding, as illustrated in. The initial structure is shown in *Figure 17(a),* while the final structure with free surfaces is shown in *Figure 17(b)* and the non-surface final structure is shown in *Figure 17(c)*. It can be seen that the grain boundary (represented by the black line), has moved similar distances in both final structures. However, the free surface structure displays more sliding than the non-surface structure, as the top grain has slid a greater distance relative to the lower grain. The GBS behavior illustrated in *Figure 17* does not fully agree with a report by Van Swygenhoven and Derlet[4], who observed that the average sliding vector is parallel to the grain boundary in specimens with parallel free surfaces, indicating that the grain can move while the boundary remains stationary. The GBS displayed in *Figure 17* clearly indicates that the grain boundary has moved while sliding has occurred. This may imply that GBS is coupled with grain boundary motion within the specimens. It was also reported in the Van Swygenhoven work that grain boundary sliding increased between grains that terminated at the free surfaces, which increased triple junction volume and

induced triple junction migration. This result is significant as it indicates that the same phenomenon may have occurred in the surface specimen examined in this work, and not in the non-surface specimen, due to its lack of free surfaces. An increase in the volume of triple junctions as well as their induced migration can potentially reduce grain boundary velocities due to triple junction drag effects[1, 35-37] . Thus, triple junction drag, due to grain boundary sliding, is a possible cause for the lower average grain boundary velocity exhibited by the surface specimen.

The grain rotation for a sample grain in the surface sample exhibits a higher angular rotation than in the non-surface sample, as illustrated in *Figure 18*. From this plot, it appears that the grain rotates more (~ −3°) in the non-surface sample than in the surface sample (~ −1.5°). The trendlines for both plots merely serve to guide the eye and are not meant to imply that the angular rotation in both the samples is proportional to $t^{-1/2}$. No definite conclusions regarding angles of rotation can be made from this data, as time constraints restricted analysis to only one grain to confirm the presence of grain rotation in the specimens. The existence of grain rotation indicates that the deformation mechanism in the nc-Ni specimens involves grain rotation in addition to grain boundary sliding.

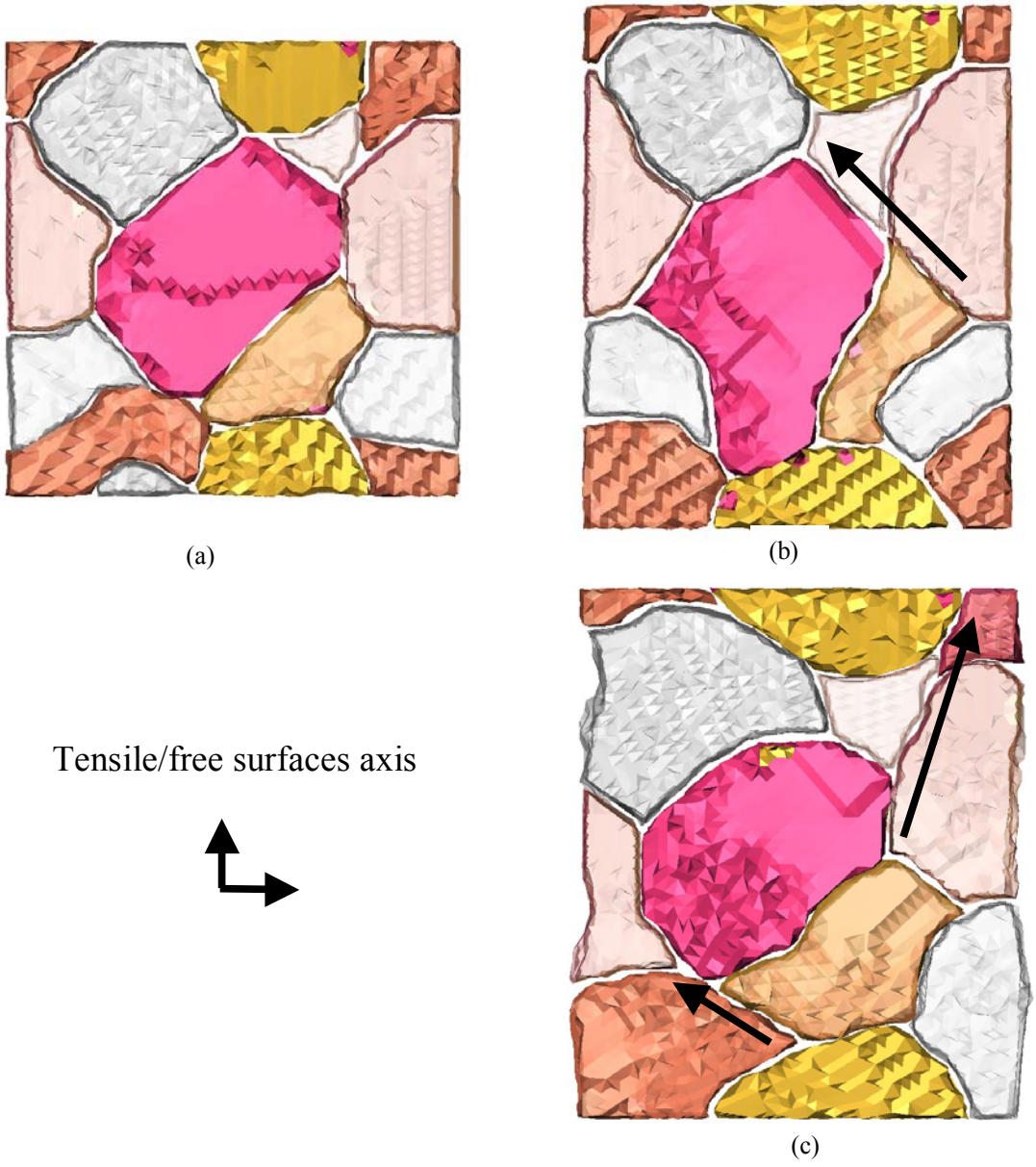

Figure 13: Deformation-driven grain boundary motion within (a) nc-Ni section (b) with no surfaces and (c) with surfaces

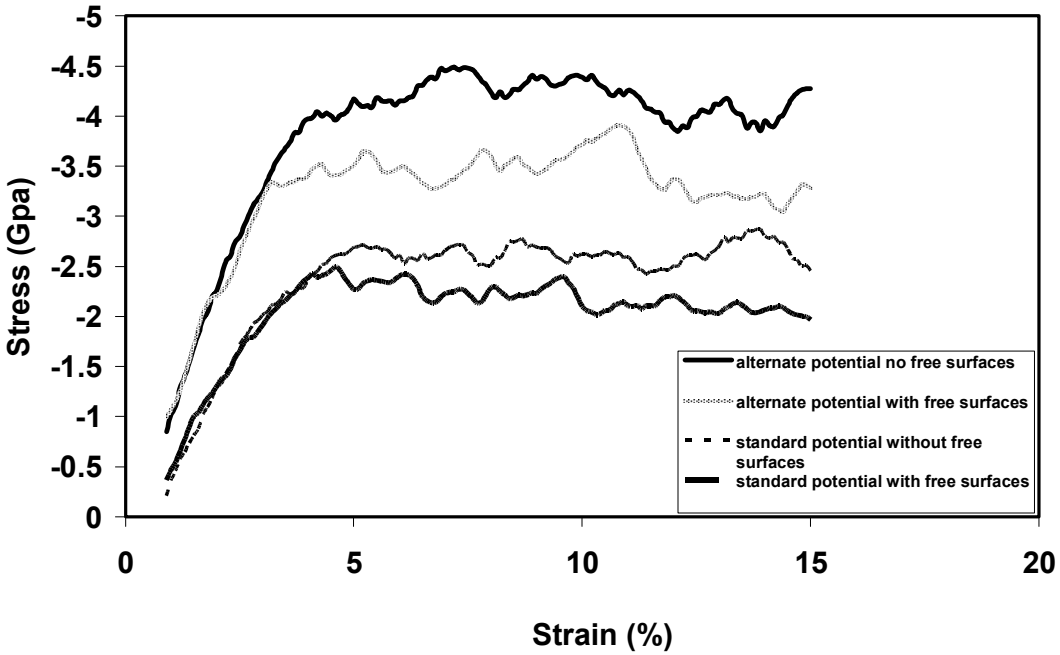

Figure 14: stress-strain curve for surface and non-surface samples governed by both potentials

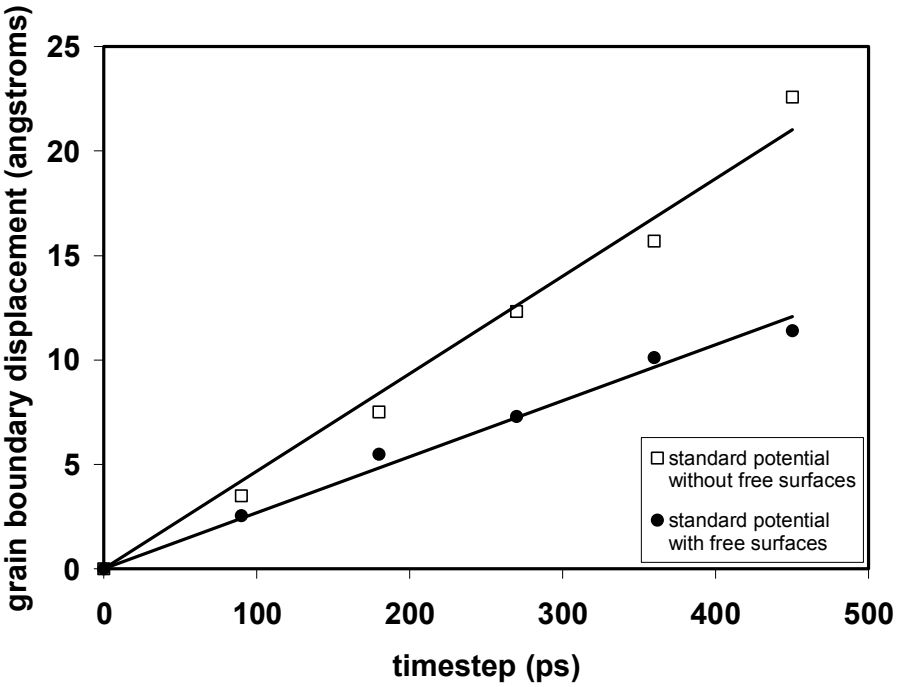

Figure 15: grain boundary displacement vs. time for a sample grain boundary in a surface and non-surface specimen

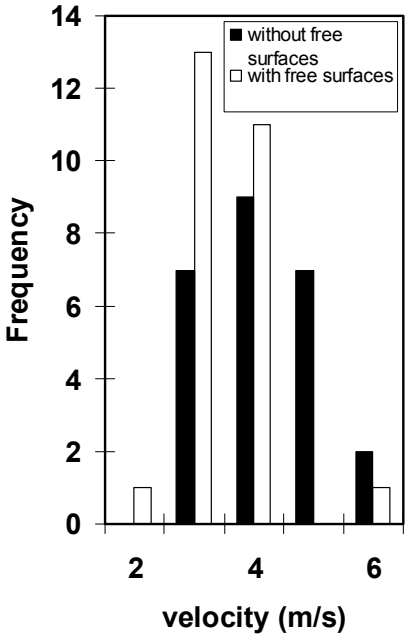

Figure 16: distribution of grain boundary velocities using the standard potential

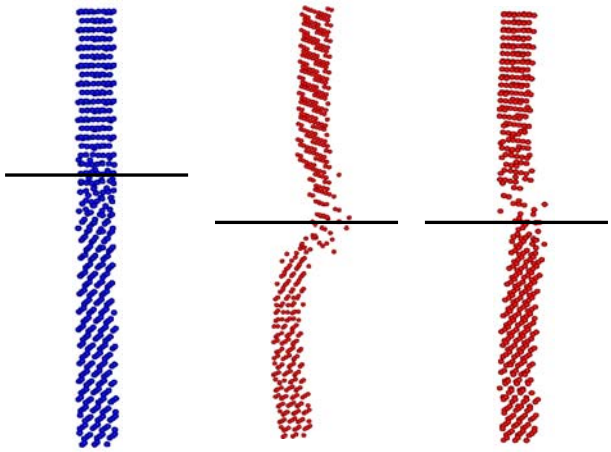

Figure 17: Grain boundary sliding in (a) initial specimen (b) final specimen (surface) and (c) final specimen (non-surface)

Table 2: average grain boundary velocity and standard deviation for surface and non-surface samples at both potentials

	Standard potential velocity (m/s), standard deviation	**Alternative Potential velocity (m/s), standard deviation**
Without Surfaces	3.63, 0.84	2.85, 0.66
With Surfaces	2.98, 0.67	1.927, 0.32

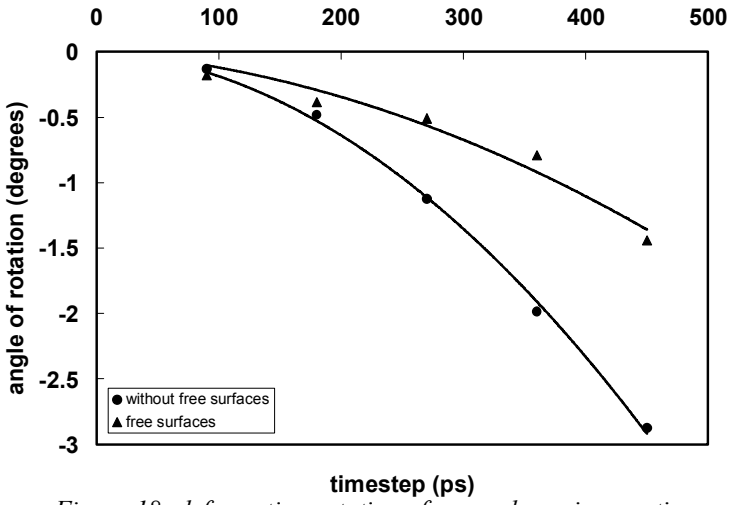

Figure 18: deformation rotation of a sample grain over time

4.1.2 Conclusion

Stress and free surface effects on nc-Ni samples were examined using MD simulations. Grain growth induced by a tensile stress is observed in the specimens. Though the exact mechanism that facilitates this growth is unknown at this time, we feel that it is likely due to grain boundary sliding and grain rotation, as both of these deformation mechanisms were present in this study. We find that surface samples exhibit a lower yield stress and a lower average grain boundary velocity than their non-surface counterparts. Both of these effects are attributed to grain boundary sliding. In our specimens, GBS occurs concurrently with grain boundary motion, which disagrees with Van Swygenhoven's observations, which indicated that grain boundary sliding occurs between two adjacent grains though the grain boundary remains stationary. However, more data must be obtained on our part to conclude that grain boundary sliding and grain boundary motion are coupled. The presence of GBS within our specimens is significant as grain boundary sliding at a surface leads to the growth and migration of triple junctions, which create drag in the specimen, and subsequently reduce the motion of grain boundary velocities in the vicinity. This is thought to be the phenomenon that resulted in a lower average grain boundary velocity for the surface samples. Grain rotation, another deformation mechanism in nc-metals, is also observed in the sample. However, present data only indicates the presence of grain rotation. Future analysis will be needed to form any well-founded conclusion concerning this phenomenon. The results of each analytical component of this work are consistent when either potential is used to govern the MD simulation, indicating that the results are independent of the

governing potential. This allows a level of confidence in the data as an accurate indicator of the phenomena that would occur in an experiment.

Future work would include examining more grains to draw conclusions concerning grain boundary sliding and angular rotation. Another phenomenon that should be closely examined is triple junction migration, as it can have drastic effects on grain boundary migration and also to verify if it occurs due to an imposed tensile stress. Lastly, simulating a different stressing mechanism on the nc-Ni samples, such as cold working followed by an anneal, would be of interest to examine the similarities and differences of nc-Ni specimens' mechanical behavior with respect to the phenomena observed under tensile loading.

4.2 Thermal Grain Growth and Grain Boundary Motion

4.2.1 Results/Discussion

Grain boundaries in any polycrystalline metal specimen contain excess energy with respect to a single-crystalline state. Thus, there is a thermodynamics driving force that reduces this energy through such mechanisms as grain-boundary area reduction or via increase in average grain size, *D*. In bulk metals, classical growth theory indicates that a single growth mechanism governs the growth rate at each length scale[3]. Such mechanisms are intrinsic grain boundary mobility, defect concentrations, and second-phase precipitates. At the nanocrystalline scale, however, the growth rate is much smaller and is unlikely that it would be controlled by the same factors as at the bulk level. The structural metamorphosis of annealing at 1300 K for 500 ps of a periodic (lacking free surfaces) nc-Ni specimen is shown in *Figure 19*. Classic grain growth phenomena occurs as it can be seen that some grains, namely the center yellow grain and the gray grains, shrink or disappear while all the other grains grow. These processes are facilitated through T1 neighbor-switching events and T2 grain boundary migration events. It can also be seen from the schematic that initially, there are 7 grains, and after the annealing treatment, 3 grains remain. This 7:3 ratio in 2-D matches closely with the 15:8 ratio found in the whole 3-D specimen (not shown here).

The average grain boundary energy is shown to have a linear relationship with $t^{1/2}$, as shown in *Figure 20*. This indicates that the change in grain boundary energy is a diffusion process. Also, it is expected that the grain boundary energy decreases with the

square root of time as grains orient themselves during annealing to achieve the lowest energy configuration, and as a result, lower the total energy of the specimen.

Grain boundaries are tracked throughout each isotherm (annealing) so that their velocities can be obtained to understand grain boundary motion behavior during an annealing process. In *Figure 21*, a sample grain boundary is tracked at the various isotherms used in the simulation. Tracking started at different timesteps for each isotherm, depending on when the specimen had attained an equilibrium grain structure. It can be clearly seen that the grain boundary displacement has a linear relationship with time at each isotherm. This linear relationship allows us to obtain the grain boundary velocity from the slope of the lines. As expected, the grain boundary velocity increases with temperature. *Figure 22* displays the grain boundary velocity distribution for the nc-Ni specimen at 1300 K. This distribution is representative of all the isotherms used in this simulation. The average grain boundary velocities and their respective standard deviations for each annealing temperature can be found in *Table 3*.

Arrhenius plots of the average grain boundary velocity-temperature relationship as well as the average energy per atom – temperature relationship illustrate whether or not the activation energy required for grain boundary motion is correlated to the activation energy needed to move a single atom in the entire specimen. As is a characteristic of an Arrhenius plot, the activation energy of a relationship is obtained from the slope of the line. As shown in *Figure 23,* the two lines are close to parallel, indicating that the two processes require similar activation energies to commence. The activation energies for the average grain boundary velocity and average energy per atom are calculated to be 53.5 kJ/mole and 54.5 kJ/mole, respectively.

Phillpot et al[34] suggest that there is a coupling between grain rotation-coalescence with grain boundary migration during grain growth. Evidently, grain coalescence annihilates the common boundary between two grains via grain rotation, resulting in two triple junctions being removed. If two triple junctions are removed than two highly curved grain boundaries are left, which induces rapid growth via grain boundary migration. They assert that a polycrystalline material will reduce excess energy stored within the grain boundaries by reducing the grain boundary area, through grain boundary migration, and also the average grain boundary energy, through grain rotation.

Since we are examining grain growth phenomena of the specimen, it was necessary to determine if normal grain growth was occurring during the annealing processes. The average grain size, *D*, was found at each timestep during an annealing treatment at 1300 K. As shown in *Figure 24* it is observed that average grain size increases linearly with time, and thus, does not follow normal grain growth. This phenomenon has been confirmed by several recent studies[1, 3, 32]. However, there is no consensus on what factor or combinations of factors are responsible for linear growth. Gottstein and Shvindlerman[1] have suggested that triple junction drag slows down grain growth in the initial stages, and causes grains to have a linear growth profile. Krill et al.[3] suggest that excess volume within grain boundaries migrate in the form of vacancies when grain boundaries are being annihilated during the reduction of grain boundary area. These vacancies severely attenuate the Gibbs free energy of the driving force, which may be grain boundary or surface energy, resulting in a linear growth profile.

The Krill study, however, may not be relevant to our work, as their growth conditions are quite different from ours. In the current study, annealing temperatures

range from 900-1450 K and annealing times range from 150-900 ps. At 1300 K, and an annealing time of 500 ps, the average grain size, *D*, ranges from 37 – 51 angstroms, as illustrated in *Figure 24*. Krill et al examined ball-milled nc-Fe specimens with annealing temperatures ranging from ~750-880 K, annealing times up to 140 min, and a resulting average grain size range of 50-250 nm. It is quite possible that different mechanisms govern grain growth in these two very different size/temperature/time regimes. Similar assertions to those of the Krill group are made in studies examining vacancy effects on grain growth kinetics by Gottstein and Shvindlerman[52, 53]. They report that parabolic growth occurs when the vacancy concentration is close to its equilibrium state. It follows then, that there is an oversaturation of vacancies, most likely within the grain boundaries. Vacancies are not observed in this simulation, possibly because they are hidden within the grain boundaries. Triple junctions are not examined in this study, either, but it is obvious that they exist in the specimen. Thus, it is possible that both of these factors contribute to the linear growth profile. According to several studies of triple junction kinetics[1, 35-37, 54], however, the triple junction drag effects decrease as the temperature increases. At the elevated annealing temperatures that have been used to grow the specimen, it is unlikely that triple junctions will be a major factor in hindering grain growth.

As in the case of mechanical deformation, grain rotation can cause grain coalescence, resulting in a single, larger grain. *Figure 25* displays the relationship between the angle of rotation for a sample grain and $t^{1/2}$ at 1300 K, thus, classifying it as a diffusion-controlled process. After 500 ps, the sample grain has rotated ~6°. Studies by Shan et al.[15] and Moldovan et al.[55] suggest that when grain rotation occurs under an

imposed torque created from the misorientation energy between grains, the periphery of the rotating grain will create some volumes of overlapping grains, while causing others to be devoid of any atoms at all, creating voids. These voids facilitate diffusional fluxes required to accommodate grain rotation. Both groups have also asserted that grain rotation does not occur in all the grains within a specimen. Grain rotation is only activated in a very small grain, or in the smallest grains in a grain-size distribution. During the process of grain rotation, adjacent grains will try to rotate themselves in such a way as to lower the grain boundary energy. The lowest possible energy orientation is $\Sigma=3$, the twin configuration. Two grains, Grain 3 and Grain 4, shown in *Figure 19*, are observed to have rotated to a quasi-twin orientation, as shown in *Figure 26*. The yellow boxes indicate the unit cell in the fcc nc-Ni.

From the attributes that are examined in this simulation, average grain boundary energy and grain rotation are the grain characteristics controlled by diffusion. The linear attributes that are examined are grain boundary velocity and the growth profile of *D*. Because all these processes are involved in grain growth, it is expected that there should be coupling mechanisms amongst the attributes. One example of such a coupling mechanism is illustrated in the Arrhenius plot shown in *Figure 23*. Average grain boundary velocity is a linear attribute whereas K, or average energy per atom, is a diffusion-controlled attribute. It may seem counterintuitive that they exhibit commensurate activation energies, in spite of having different time-dependencies. However, it should be noted that although motion of an entire grain boundary is shown to have a linear relationship with time, the atoms within the grain boundary still move by jumps through the lattice, and thus, move via diffusion. Thus, grain boundary motion and

average energy per atom are both controlled by diffusion, and thus, exhibit equivalent activation energies.

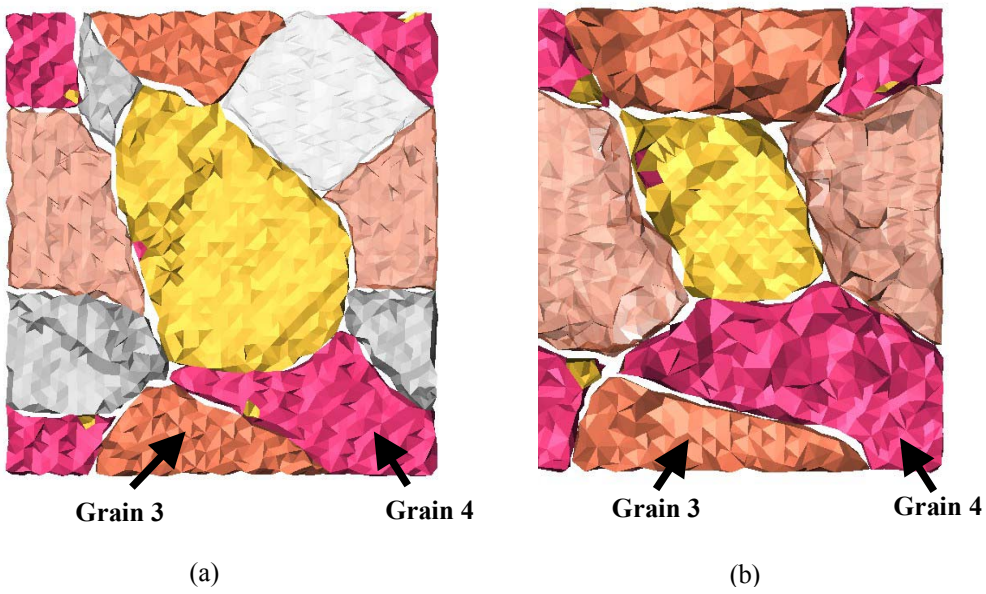

Figure 19: grain growth in (a) nc-Ni specimen (b) after an anneal at 1300 K for 500 ps

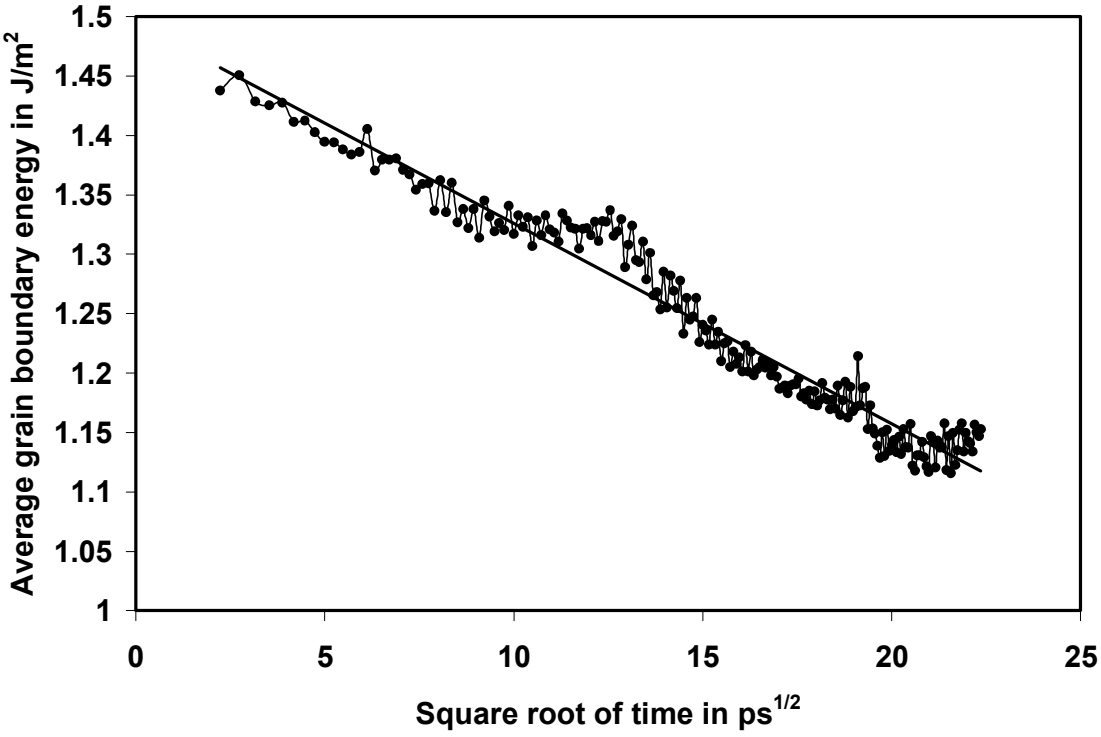

Figure 20: average grain boundary energy vs. square root of time

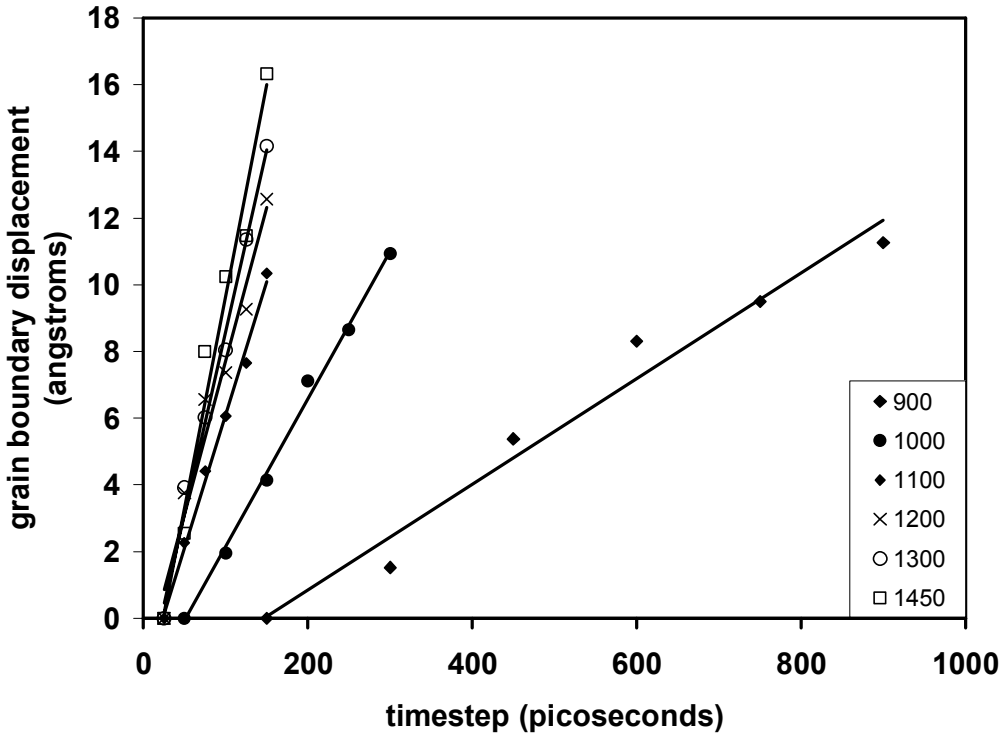

Figure 21: grain boundary displacement vs. time profiles for a sample grain boundary at various annealing temperatures

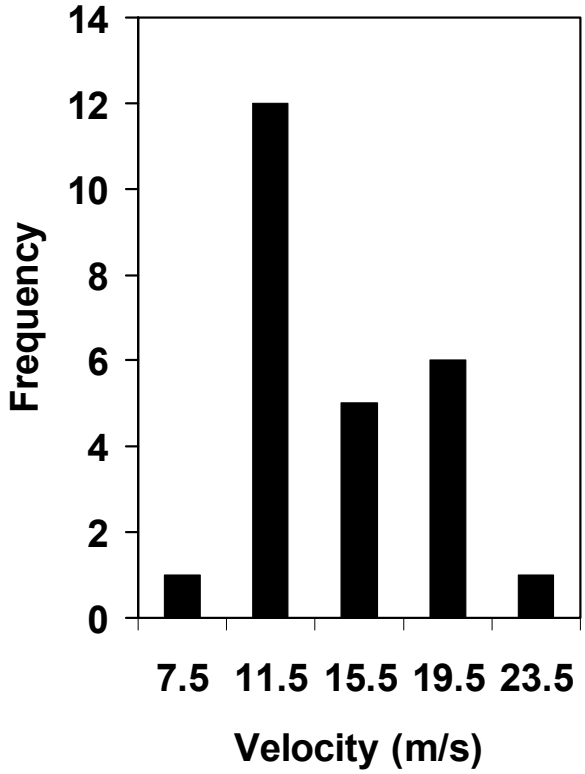

Figure 22: distribution of grain boundary velocities at 1300 K

Table 3: average grain boundary velocities and associated standard deviations for each annealing tempature

Temperature (K)	Average Velocity (m/s), standard deviation
900	1.252, 0.394
1000	3.610, 1.011
1100	8.500, 2.041
1200	10.711, 2.414
1300	12.639, 3.627
1450	21.146, 7.992

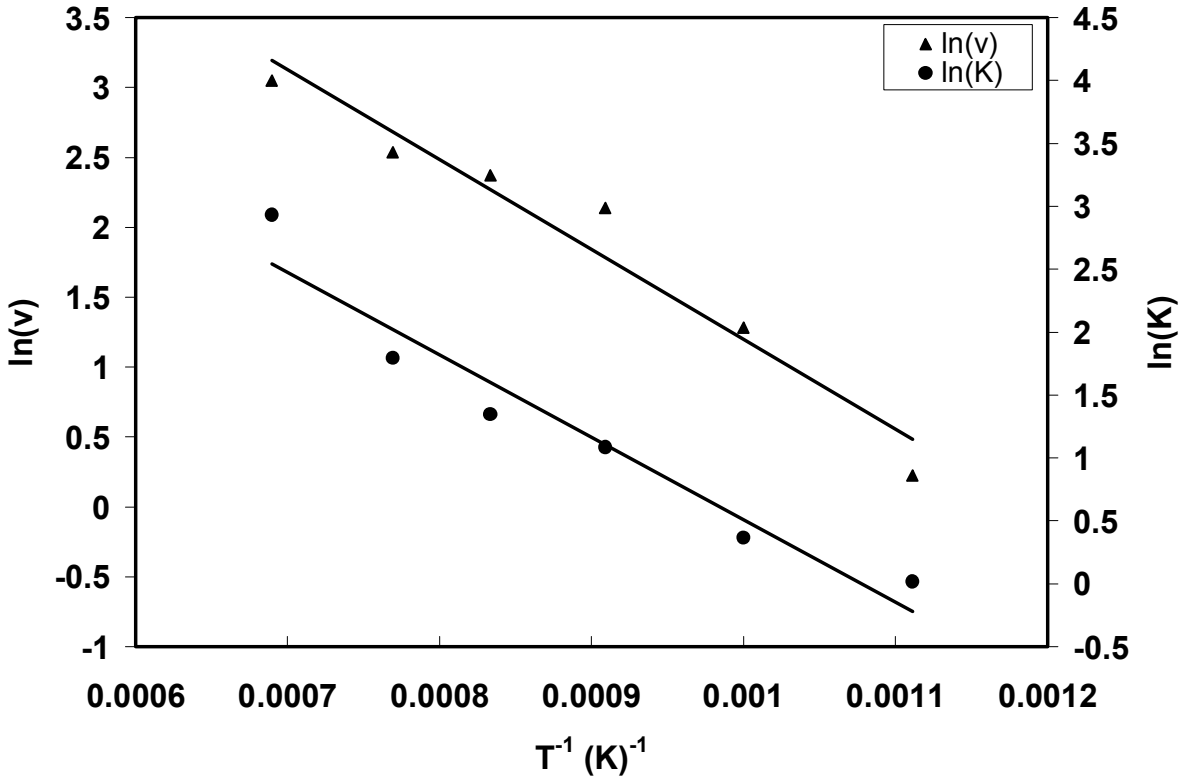

Figure 23: Arrhenius plot of the natural log of both the grain boundary velocity and the energy per atom in the specimen vs. the reciprocal of the temperature

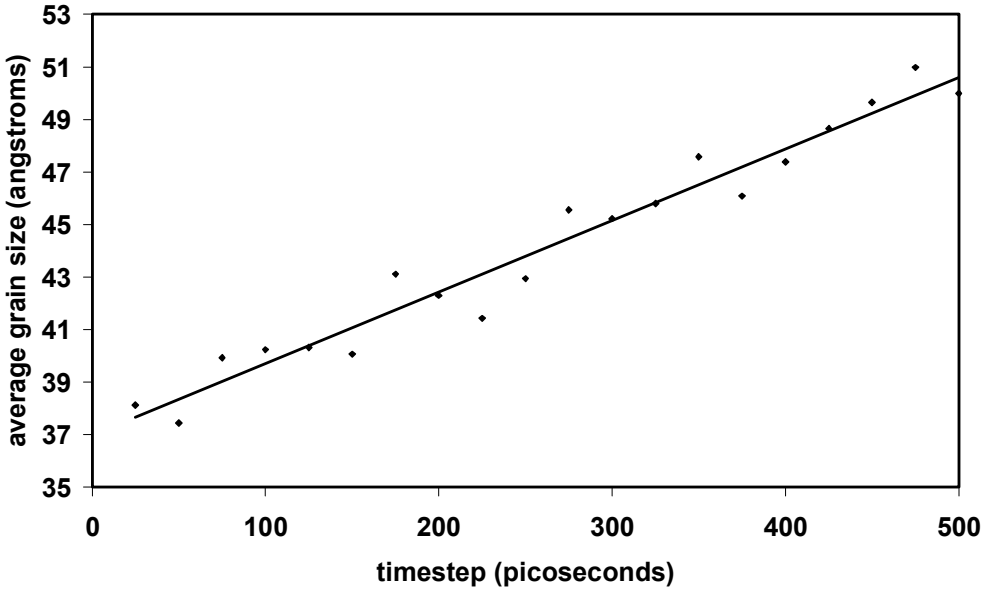

Figure 24: average grain size vs. timestep at 1300 K

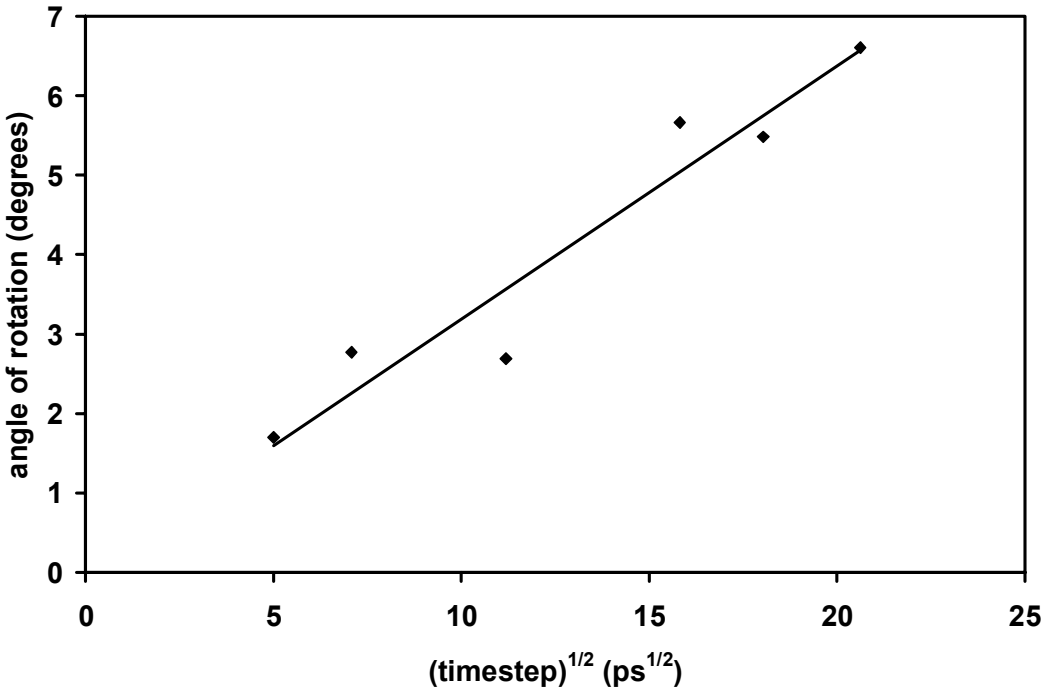

Figure 25: angle of rotation of a sample grain vs. time

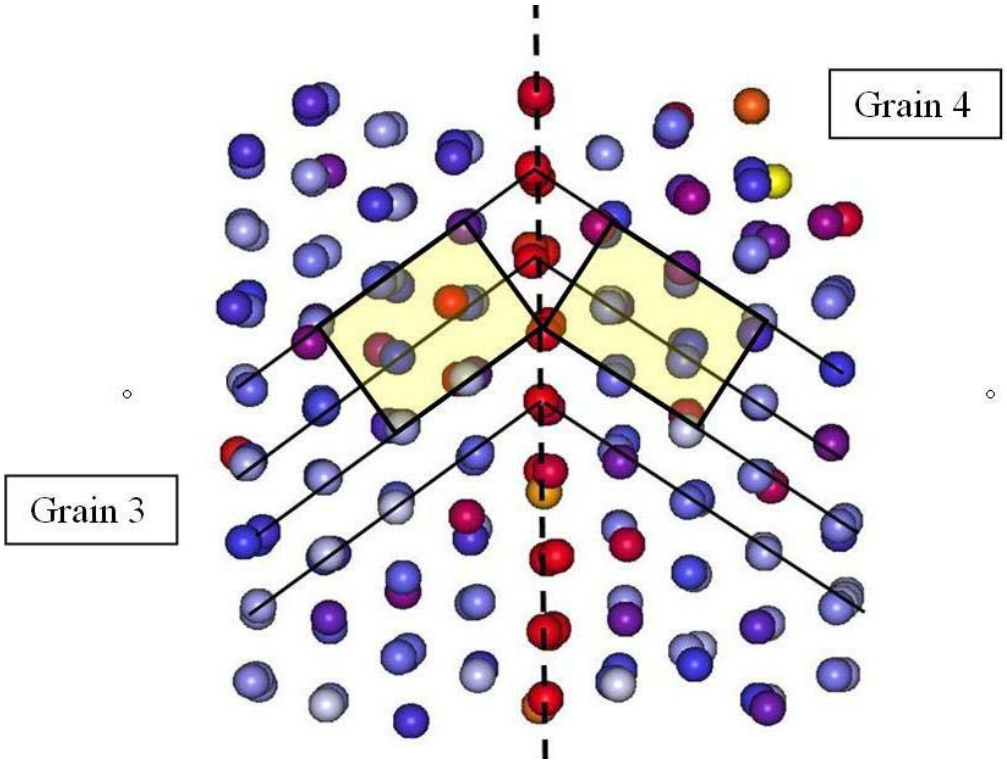

Figure 26: Two grains, Grain 3 and Grain 4, have rotated during the anneal to form a twin. The yellow boxes display the unit cell for fcc nc-Ni

4.2.2 Conclusions

Thermal grain growth appears to exhibit classical grain growth phenomena in which some grains will grow at the expense of others, via T1 and T2 events. During an annealing process, the average grain boundary energy decreases with $t^{-1/2}$, as grains seek to orient themselves in a lower-energy configuration with their neighbors via rotation. The specimen as a whole seeks to lower its total energy through grain-growth coalescence, which involves adjacent grains rotating into the same orientation to remove the grain boundary, creating a larger, single grain bounded by high angle grain boundaries. This results in rapid growth of the grain through grain boundary migration. Average grain boundary velocities were found to increase with temperature, as expected. Grain boundary motion and average energy per atom are attributes that exhibit equivalent activation energies. This is attributed to the fact that they both involve the movement of atoms, which are transported through the specimen via diffusion. Grain rotation analysis performed on one grain shows that grain rotation is diffusion-controlled.
Grain growth at such small sizes, such as an average grain size, $D \sim 5$ nm at an annealing temperature of 1300 K, is found to be linearly dependent upon time. This may be caused by vacancies or triple junction effects. However, because specimens are grown at elevated temperatures, it is not expected that triple junction drag effects will have any affect on grain growth. .

Future work should include more samples for grain rotation analysis. Several studies have indicated that grain rotation does not occur in all grains within a sample. This has implications on thermal grain growth, as grain-growth coalescence is a major grain growth mechanism.

Appendix A: Tensile Stress Effects on Grain Boundary Motion

Grain Boundary Velocity Distributions

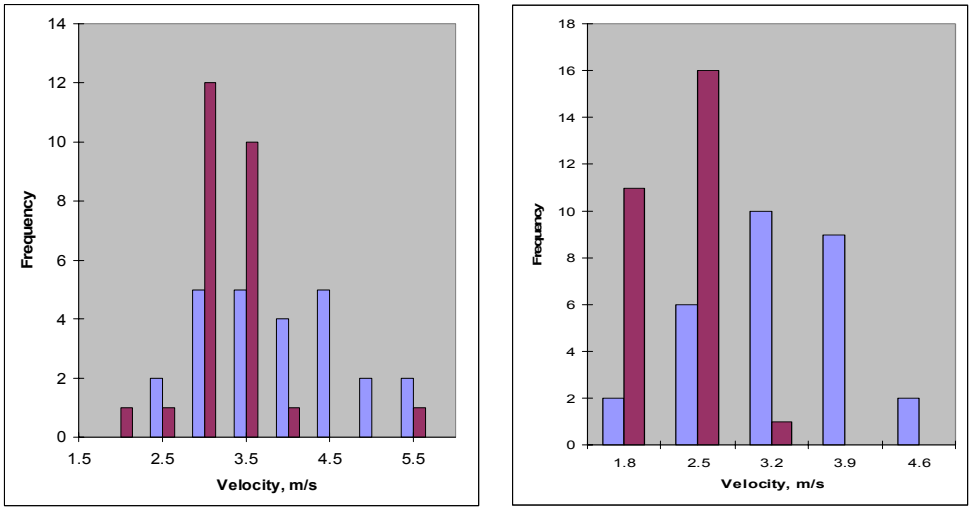

Figure 27: frequency histogram of the grain boundary velocities using (a) standard potential without surfaces (blue) and with surfaces (red) and with (b) the alternate potential without surfaces (blue) and with surfaces (red)

Grain Boundary Sliding

In addition to the GBS shown in *Figure 28*, GBS was observed in other specimens, as well. It should be noted, that there has still not been enough data collected to make concrete conclusions concering GBS within our specimens. As shown in *Figure 28*, the final non-surface structure (c) has exhibited higher grain boundary motion as the grain boundary (in black) has moved a distance greater than that of the final free surface structure (b). From this figure, however, it is not clear if GBS has occurred. It should be noted that the grain boundary has not moved in the final free surface structure with respect to the initial structure.

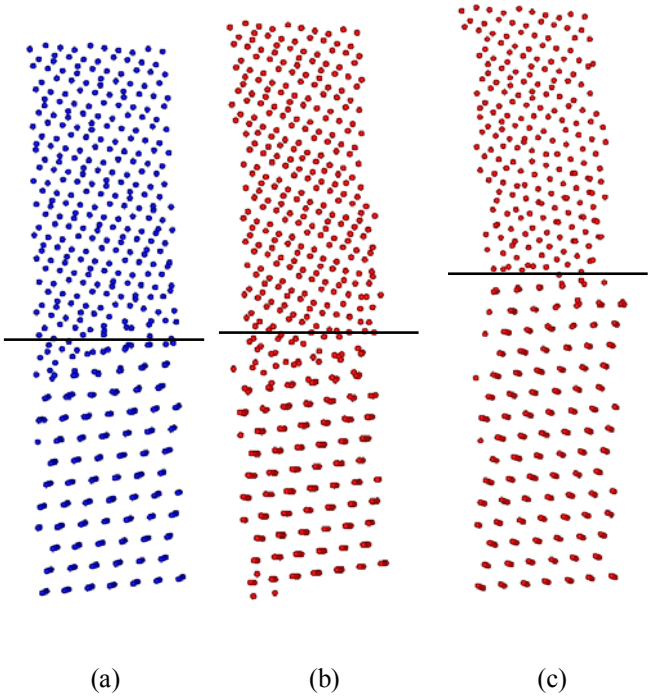

Figure 28: grain boundary sliding in (a) an initial structure, in a (b) final structure with surfaces, and in a (c) final structure without surfaces

It can be seen that the major distinction between the specimens shown in *Figure 29* is that sliding vectors in the surface specimen (*Figure 298 (b)*) are parallel to the grain

boundary (black lines), while in the non-surface sample (*Figure 29 (a)*) they are not, agreeing with Van Swygenhoven's work[5]. However, a peculiarity in *Figure 29* is that the displacement vectors shown in both samples indicate that the atoms in the grain have moved several atomic lengths away from their original positions, whereas they were expected to move only one or two atomic lengths.

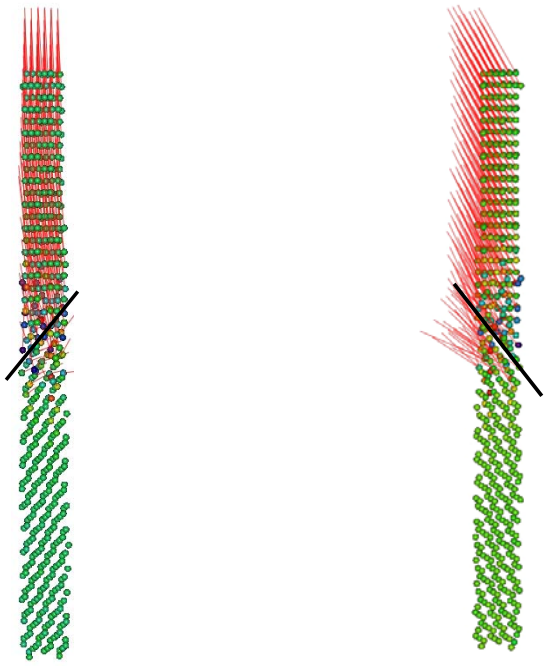

Figure 29: Grain boundary sliding in (a) non-surface specimen and (b) surface specimen.

Appendix B: Thermal Effects on Grain Boundary Motion

Data for Sample Grain Boundary B-G Tracked at Each Isotherm

movement of B-G	**900**	**velocity (m/s)**
abs. distance, sum	t	
0	0	
0	150	
1.525042133	300	
5.382817945	450	
8.304492277	600	
9.490511115	750	
11.25771534	900	**1.501028712**

movement of B-G	**1000**	
abs. distance, sum	t	
0	0	
0	50	
1.955007577	100	
4.145755471	150	
7.11934368	200	
8.641793324	250	
10.93655528	300	**4.374622111**

movement of B-G	**1100**	
abs. distance, sum	t	
0	0	
0	25	
2.273329054	50	
4.421507718	75	
6.059979066	100	
7.652938863	125	
10.34904885	150	**8.279239081**

movement of B-G	**1200**
abs. distance, sum	t
0	0
0	25
3.762742814	50
6.563106488	75
7.368647141	100

9.268155268	125	
12.56807108	150	**10.05445687**

movement of B-G	**1300**	
abs. distance, sum	t	
0	0	
0	25	
3.91470464	50	
6.025121217	75	
8.038824163	100	
11.35878391	125	
14.15461498	150	**11.32369198**

movement of B-G	**1450**	
abs. distance, sum	t	
0	0	
0	25	
2.551150475	50	
7.993001129	75	
10.23271061	100	
11.47846067	125	
16.32328968	150	**13.05863174**

Grain Boundary Velocity Distributions at Each Isotherm

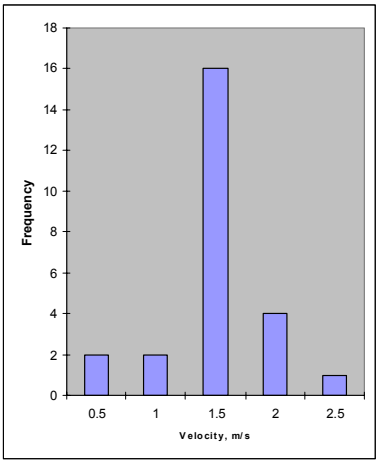

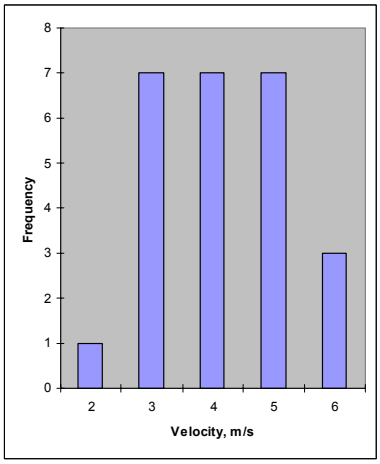

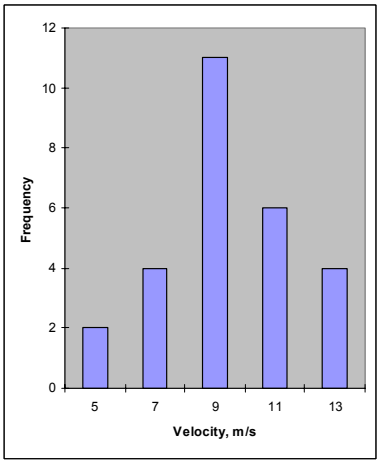

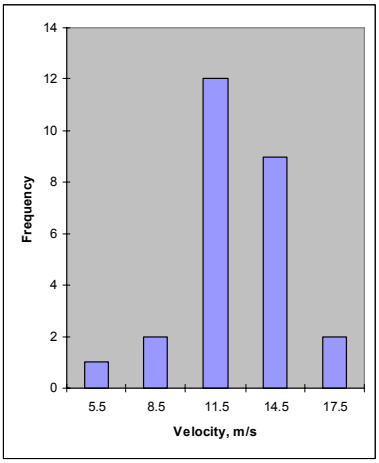

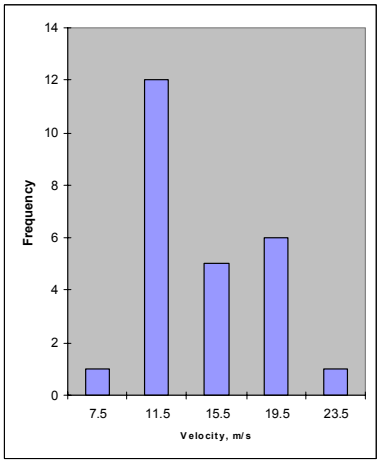

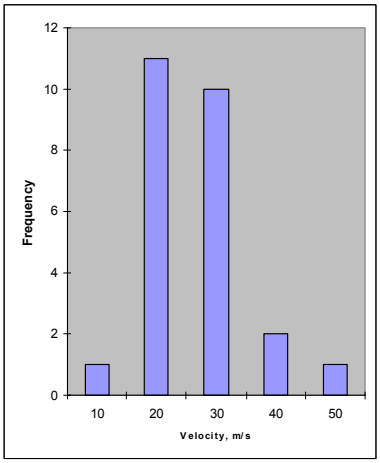

Grain Growth – Intercept Method

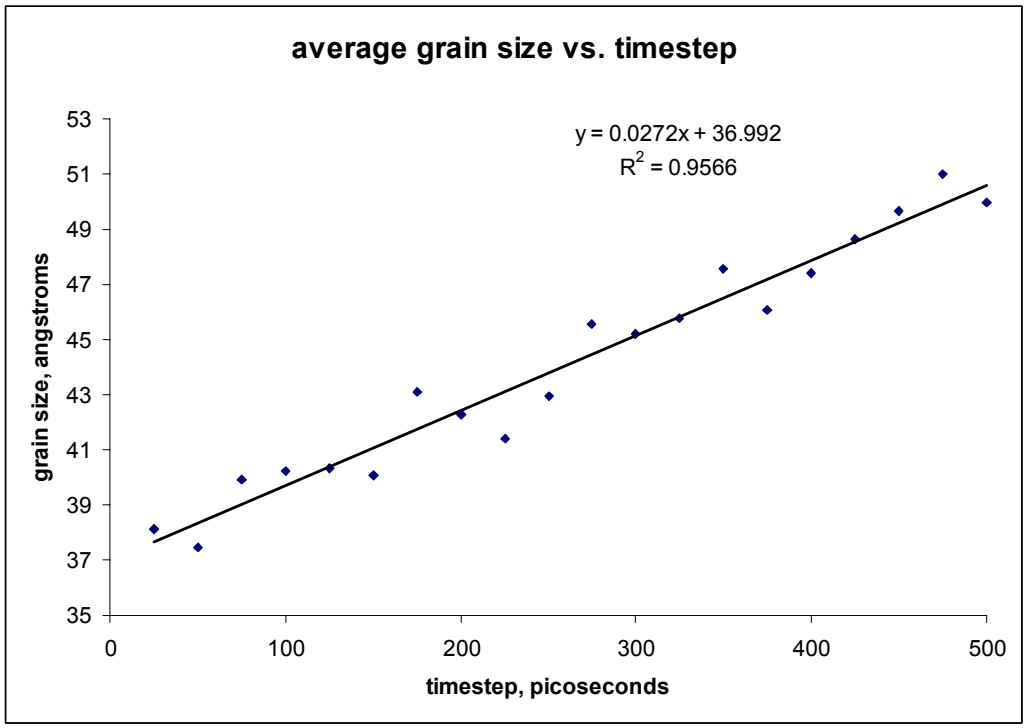

Figure 30: average grain growth at 1300 K with linear function

timestep	sqrt timestep	averages	avg - 38
25	5	38.1247126	0.124712603
50	7.071067812	37.44309277	-0.556907229
75	8.660254038	39.92675912	1.926759119
100	10	40.23664463	2.236644632
125	11.18033989	40.31952923	2.319529228
150	12.24744871	40.06431298	2.064312976
175	13.22875656	43.10888071	5.108880713
200	14.14213562	42.30062447	4.300624468
225	15	41.43290281	3.432902807
250	15.8113883	42.93956593	4.939565933
275	16.58312395	45.55492567	7.554925674
300	17.32050808	45.2268599	7.226859902
325	18.02775638	45.79291668	7.792916676
350	18.70828693	47.57161897	9.571618972
375	19.36491673	46.07879527	8.078795271
400	20	47.38503077	9.385030768
425	20.61552813	48.65194422	10.65194422
450	21.21320344	49.64666036	11.64666036
475	21.79449472	50.97890017	12.97890017
500	22.36067977	49.98872002	11.98872002

References

1. Gottstein and Shvindlerman, Journal of Materials Science, 2005. 40: p. 819-839.
2. Kumar, Van Swygenhoven, and Suresh, Acta Materialia, 2003. 51: p. 5743-5774.
3. Krill, Physical Review Letters, 2001. 86: p. 842-845.
4. Van Swygenhoven and Derlet, Philosophical Magazine A, 2002. 82: p. 1-15.
5. Hou, Kharlamov, and Zhurkin, Physical Review B, 2002. 66: p. 195408-1 - 195408-14.
6. Keblinski, Wolf, Phillpot, and Gleiter, Scripta Materialia, 1999. 41: p. 631-636.
7. Keblinski, Wolf, Phillpot, and Gleiter, Philosophical Magazine A, 1999. 79: p. 2735-2761.
8. Van Swygenhoven, Science, 2002. 296: p. 66-67.
9. Kumar, Suresh, Chisholm, Horton, and Wang, Acta Materialia, 2003. 51: p. 387-405.
10. Shan and Ma, Advanced Engineering Materials, 2005. 7: p. 603-606.
11. Pande and Masamura, Materials Science & Engineering A, 2005. 409: p. 125-130.
12. Reed-Hill and Abbaschian, *Physical Metallurgy Principles*. 3rd ed. 1992, Boston: PWS-KENT Publishing Company. 256-261.
13. Ovid'ko, Science, 2002. 295: p. 2386.
14. Murayama, Howe, Hidaka, and Takaki, Science, 2002. 295: p. 2433-2435.
15. Shan, Stach, Wiezorek, Knapp, Follstaedt, and Mao, Science, 2004. 305: p. 654-657.
16. Chen and Yan, Science, 2005. 308: p. 356c.
17. Shan, Stach, Wiezorek, Knapp, Follstaedt, and Mao, Science, 2005. 308: p. 356d.
18. Schiotz, Materials Science & Engineering A, 2004. 375-377: p. 975-979.
19. Schiotz, Nature, 1998. 391: p. 561-563.
20. Van Swygenhoven and Derlet, Physical Review B, 2001. 64: p. 224105-1 - 224105-9.
21. Hemker, Science, 2004. 304: p. 221-222.
22. Chen, Ma, Hemker, Sheng, Wang, and Cheng, Science, 2003. 300: p. 1275-1277.
23. Embury, *Twinning in advanced materials*. in *Materials Week*. 1994. Pittsburgh, PA: TMS.
24. Zhu, Liao, Srinivasan, Zhao, Baskes, Zhou, and Lavernia, Applied Physics Letters, 2004. 85: p. 5049-5051.
25. Zhu and Langdon, Materials Science & Engineering A, 2005. 409: p. 234-242.
26. Bigot and Champion, NanoStructured Materials, 1998. 10: p. 1097-1110.
27. Van Swygenhoven, Derlet, and Froseth, Applied Physics Letters, 2004. 85: p. 5863-5865.
28. Van Swygenhoven, Derlet, and Froseth, Advanced Engineering Materials, 2005. 7: p. 16-20.
29. Jin, Minor, Stach, and Morris, Acta Materialia, 2004. 52: p. 5381-5387.
30. Callister, W.D., *Materials Science and Engineering: An Introduction*. 5th ed. 2000, New York: John Wiley & Sons, Inc.
31. Mould and Cotterill, *Recrystallization and Grain Growth in Metals*. 1976, New York: John Wiley & Sons.

32. Iordache, Whang, Jiao, and Wang, NanoStructured Materials, 1999. 11: p. 13430-1349.
33. Moldovan, Yamakov, Wolf, and Phillpot, Physical Review Letters, 2002. 89: p. 206101-1 - 206101-4.
34. Phillpot, Wolf, Haslam, Moldovan, and Gleiter, Materials Science & Engineering A, 2001. 318: p. 293-312.
35. Gottstein, Mattissen, Shvindlerman, and Molodov, Acta Materialia, 2005. 53: p. 2049-2057.
36. Gottstein and Shvindlerman, Acta Materialia, 2002. 50: p. 703-713.
37. Novikov, Scripta Materialia, 2005. 52: p. 857-861.
38. Wang, Cheng, Wei, Ma, Nieh, and Hamza, Scripta Materialia, 2004. 51: p. 1023-1028.
39. Van Swygenhoven, Derlet, and Hasnaoui, Acta Materialia, 2002. 50: p. 3927-3939.
40. Hyde, B., *Effects of Carbon on Fracture Mechanisms in Nanocrystalline BCC Iron - Atomistic Simulations*, in *Materials Science and Engineering*. 2004, Virginia Tech.
41. Dawes and Baskes, Physical Review B, 1984. 29: p. 6443-6453.
42. Voter and Chen, *MRS Symposia Proceedings*. 1987.
43. Mishin and Farkas, Physical Review B, 1999. 59: p. 3393.
44. Plimpton, S.J., Journal of Computational Physics, 1995. 117: p. 1-19.
45. Valadon, P., *RasTop* 2004.
46. *Amira*. 2004, Mercury Computer Systems
47. Budrovic, Van Swygenhoven, Derlet, Petegem, and Schmitt, Science, 2004. 304: p. 273-276.
48. Clark and Alden, Acta Metallurgica, 1973. 21: p. 1195.
49. Friedez, Adv Ceram, 1985. 10: p. 720.
50. Wolf, Moldovan, Yamakov, Phillpot, and Gleiter, Acta Materialia, 2003. 51: p. 2097-2112.
51. Van Swygenhoven, Derlet, and Hasnaoui, Physical Review B, 2002. 66: p. 184112-1 - 184112-8.
52. Gottstein, Shvindlerman, and Estrin, Acta Materialia, 1999. 47: p. 3541-3549.
53. Gottstein, Shvindlerman, and Estrin, and Rabkin, Scripta Materialia, 2000. 43: p. 141-147.
54. Nazarov, Bachurin, Shenderova, and Brenner, Materials Science & Engineering A, 2003. 359: p. 247-252.
55. Moldovan, Wolf, and Phillpot, Acta Materialia, 2001. 49: p. 3521-3532.
56. Srolovitz and Mendelev, Modelling Simul. Mater. Sci. Eng., 2002. 10: p. R79-R109.